Invited review: Infrared spectroscopy of planetary atmospheres: Searching for insights into their past and present histories

Thérèse Encrenaz

Invited review: Infrared spectroscopy of planetary atmospheres : Searching for insights into their past and present histories

Thérèse Encrenaz
LESIA, Observatoire de Paris – PSL, CNRS, France

Gerard P. Kuiper Prize Lecture, AAS-DPS General Assembly, October 2021

Submitted to Icarus, November 30th, 2021
Revised, December 30th, 2021

Corresponding author:
Thérèse Encrenaz
LESIA, Paris Observatory, 5 place Janssen 92195 Meudon, France
Therese.encrenaz@obspm.fr

Abstract

This article reflects my personal experience and illustrates some developments in the field of planetary spectroscopy, achieved within the Planetology Group of Paris Observatory over the past fifty years. Over these decades, planetary spectroscopy has led to the identification of minor atmospheric species with mixing ratios as low as a few parts per billion (ppbv). Since the early 1970s, we have been measuring infrared spectra of giant planets and their satellites, in order to search for new minor species and to determine elemental and isotopic ratios, for better constraining their formation and evolution processes. In particular, observations of Jupiter at the time of the Shoemaker-Levy 9 collision, in 1994, allowed us to monitor the thermal sequence and the formation of stratospheric water vapor; a few years later, spectra taken by the Infrared Space Observatory confirmed the presence of an external oxygen source in all giant planets and Titan. More recently, the advent of bi-dimensional infrared arrays has allowed us to map the distribution of these components over planetary disks, and to use them as tracers of dynamical and photochemical processes. In complement to in-orbit observations recorded by space missions, high-resolution spectral mapping from the ground allows us to obtain instantaneous global maps of the planets, and thus to trace transient phenomena or temporal variations of minor atmospheric species over short and long timescales. Over the past twenty years, we have been monitoring the behavior of minor atmospheric species on Mars and Venus, using the TEXES (Texas Echelon Cross Echelle Spectrograph) at the NASA IRTF (InfraRed Telescope Facility) at Maunakea Observatory, and the EXES (Echelon Cross Echelle Spectrograph) aboard SOFIA (Stratospheric Observatory For Infrared Astronomy): H_2O_2 and H_2O on Mars, D/H on Mars, SO_2 and H_2O at the cloud top of Venus. In addition, in an attempt to build a 3-D image of the sulfur and water cycles on Venus, we have obtained maps of SO, SO_2 and HDO in its upper mesosphere (about 20 km above the cloud top) using the ALMA (Atacama Large Millimeter/submillimeter Array) facility in Chile. These observations are presented and discussed in the light of global dynamical and photochemical models, and interpreted in the context of the past and present history of these planets. In the conclusion, I present the perspectives of this work for the forthcoming development of exoplanetary spectroscopy.

Key words: Atmospheres, evolution; Jupiter, atmosphere; Mars, atmosphere; Venus, atmosphere

1. Introduction

Infrared spectroscopy of planets is ideally suited for studying the composition of their neutral atmospheres. Indeed, the infrared range is the region where the strongest spectral signatures of neutral molecules are found, in the form of rotational bands or vibration-rotation bands, while transitions associated with radicals, ions or atoms, corresponding to higher energies, are found in the visible and ultraviolet range. In addition, the thermal emission of solar-system planets is maximum in the infrared range.

Considerable progress has been achieved in the domain of planetary spectroscopy over the five past decades. This is illustrated, in the case of Jupiter, by a comparison between an infrared spectrum recorded by F. C. Gillett and his team in 1969, and the spectrum recorded by the Short Wavelength Spectrograph (SWS) of the Infrared Space Observatory (ISO: www.cosmos.esa.int/web/iso) in 1996 (Figure 1). In the 1960s, only ground-based spectrophotometric measurements could be obtained in the thermal infrared range, with the use of circular variable filters providing a spectral resolving power of about 50.

The Jupiter spectrum recorded in 1969 already reveals important features. As for all solar system objects, the spectrum shows two components, the solar reflected radiation which peaks at 0.5 μm, and the thermal emission of the planet that dominates in the mid-infrared range. In the first case, the signatures of atmospheric components appear in absorption in front of the solar continuum. In the second case, they appear either in emission or in absorption, depending on the region probed: emission lines appear in the stratosphere (where the temperature increases with altitude) while tropospheric lines (formed in a region below where the temperature decreases as the altitude increases) are in absorption (see e.g. Hanel et al. 2003). The spectrum recorded by Gillett et al. (1969) shows a strong thermal continuum in the 5-μm window where the lower troposphere of Jupiter can be probed, and an emission at 7.7 μm attributed to methane, showing evidence for a temperature inversion above the tropopause. However, no specific identification of individual molecule could be made, as such an assessment requires a higher spectral resolution. This analysis became possible with the development of Fourier-Transform spectrometers and grating spectrometers. The Jupiter spectrum recorded in 1996 by ISO-SWS corresponds to a spectral resolving power of about 2000, sufficient to resolve the molecular bands, either in absorption (in the troposphere, around 5 μm and 10 μm) or in emission (in the stratosphere, around 7.7 μm and 12 μm).

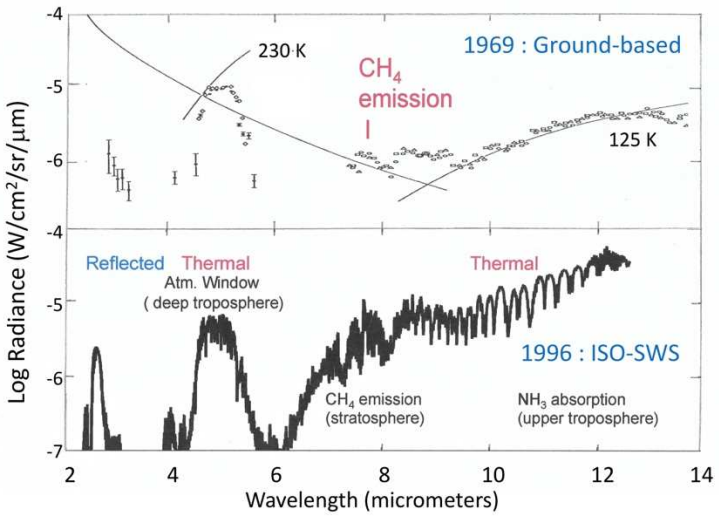

Figure 1. *Top: The spectrum of Jupiter recorded from the ground by Gillett et al. (1969), with a spectral resolving power of 50. The black curves indicate the reflected solar component (below 8 µm), and blackbodies at 230 K (around 5 µm) and. 125 K (above 8 µm). Bottom: the same spectrum recorded by the Short Wavelength Spectrometer of the Infrared Space Observatory in 1996 with a spectral resolving power of about 2000. Sources: Gillett et al. 1969 (top), Encrenaz et al. 2003 (bottom).*

In addition to the intrinsic information about Jupiter, the spectrum recorded by Gillett et al. (1969) is interesting, as it more or less corresponds to what we can observe today on the brightest exoplanets, mostly with the use of the Spitzer telescope. Its comparison with higher-resolution spectra from ISO thus allows us to imagine the enhanced quality of spectra that we may hope to get for exoplanets in the thermal infrared in the future.

The purpose of this article is to present a personal and biased illustration of some developments that have been achieved at Paris Observatory (www.observatoiredeparis.psl.eu) in the field of planetary spectroscopy over the past fifty years, following the progress realized in the development of infrared detectors, spectrometers and telescopes. The first part (Section 2) describes giant planet observations, starting with the spectrum of Jupiter in the 10-µm window (2.1), the monitoring of the SL9-Jupiter collision in 1994 (2.2), and the ISO observations in the late 1990s (2.3), followed by ground-based observations of Uranus and Neptune in the 2000s at the InfraRed Telescope Facility (IRTF) at the Maunakea Observatories (www.maunakeaobservatories.org) and the Very Large Telescope (VLT: www.eso.org/public/teles-instr/paranal-observatory/) in Cerro Paranal, Chile (2.4 and 2.5), leading us from disk-integrated spectra to spectral mapping. The second part of this article (Section 3) is mostly devoted to the spectral mapping of Mars (3.1) and Venus (3.2), achieved with the TEXES thermal imaging spectrometer at the IRTF over the past twenty years. Section 4 presents a brief review of planetary spectroscopy's main contributions, a discussion about some remaining open questions, and finally some perspectives about exoplanetary spectroscopy.

2. Giant planets

Until the beginning of the XXIst century, in most cases, infrared planetary spectroscopy was achieved with single detectors, and disk-integrated spectra of planets were recorded. In the case of the giant planets, infrared spectroscopy had two main objectives: (1) identify minor species to better understand the physico-chemical processes at work in these atmospheres, and (2) determine elemental and isotopic abundance ratios in the giant planets to better constrain their formation scenario. Indeed, in the 1970s and 1980s, two possible formation models were proposed: (1) the direct collapse model, in which the giant planets are formed by gravitational instability from the direct collapse of matter within the protosolar disk (Cameron 1973, 1988; Cameron & Pine 1973), and (2) the core-accretion model, in which the protosolar matter is accreted around a solid core, mostly made of ice, whose mass is in the range of 10-15 terrestrial masses (Mizuno, 1980; Pollack et al. 1996). Elemental and isotopic ratios are an excellent diagnostic to discriminate between these two models; indeed, no enrichment versus hydrogen with respect to the solar nebula is expected in the first case, while an enrichment is expected in the second case, due to the high content of the heavy elements in the ices. The larger the mass fraction of the icy core in the giant planet, the stronger the enrichment is (in the case of exoplanets, we now use the term of "metallicity", by analogy with the stars). Assuming a core mass of 10 terrestrial masses, a simple calculation (Owen & Encrenaz 2006) shows that the expected enrichment is about 3-4 for Jupiter (core mass fraction of 3%), 7-9 for Saturn (core mass fraction of 10%) and above 30 for Uranus and Neptune (core mass fraction > 50%); the uncertainty reflects a variation with time in the choice of the elemental abundance values in the Sun. However, it must be kept in mind that there are underlying assumptions in this calculation; in particular, the volatile elements in the ices are assumed to be homogeneously mixed with the external layers of the planet during the collapse and post-collapse phases of the planet's formation. As shown by the results of the Juno probe regarding the internal structure of Jupiter (Guillot 2019), the assumption of an initial icy core of ten terrestrial masses is clearly oversimplified. Nevertheless, possibly as a result of a fortuitous coincidence, the enrichments measured in the giant planets happen to be consistent with the predictions of this simple model (Owen & Encrenaz 2006).

Among the elemental ratios, the easiest one to be measured with infrared spectroscopy is C/H, which can be directly inferred from the CH_4/H_2 ratio. In the case of Jupiter and Saturn, methane is uniformly distributed with altitude and over the disks, and its spectral signatures are present everywhere over the infrared spectrum. Another key element is the D/H ratio. Deuterium was initially formed in the Big Bang and is continuously destroyed in stars through stellar nucleosynthesis. In the case of the gaseous giants, mostly made of their protosolar gas, the D/H ratio should reflect its value in the protosolar nebula (expected to be intermediate between the primordial value and its present value, measured in the local interstellar medium). In contrast, D/H is expected to be enriched in the icy giants, because, as observed in the interstellar medium as well as in the laboratory, deuterated species are known to be enriched in ices, as an effect of ion-molecule reactions. Thus, the D/H ratio can be used as an indicator of the formation temperature: the larger the ratio, the colder is the formation environment; in particular, the measurement of D/H in water has been widely used for constraining the origin of comets (Encrenaz 2008). In the giant planets, D/H can be measured either from HD/H_2 or CH_3D/CH_4 and we attempted both methods in the case of Jupiter.

In the 1970s, HD transitions had been detected in the reflected solar component of the Jupiter spectrum, but their interpretation was difficult, due to the effect of scattering in the radiative transfer. With Toby Owen (SUNY, Stony Brook) and Michel Combes (Paris Observatory), we

used an indirect method to minimize as much as possible the scattering effects. We selected weak transitions of HD and CH_4 of comparable intensities, close in wavelength, and we directly estimated the HD/CH_4 ratio (hence the D/C ratio) from the intensity ratio of these two transitions. Using an independent measurement of C/H, we inferred a D/H ratio of about 2.3 +/-1.1 10^{-5} (Combes et al. 1978; Combes and Encrenaz 1979).

Twenty years later, the use of ISO made possible the direct measurement of HD in the far infrared range on the four giant planets (see below, 2.3), confirming our earlier estimate. In the late 1990s, the mass spectrometry in-situ measurements of the Galileo probe definitely favored the core-accretion model (Owen et al. 1999).

2.1 Jupiter in the 10μm window

In the early 1970s, there was no existing instrument capable of measuring the mid-infrared spectrum of Jupiter with enough spectral resolution to separate the molecular components of the planet's atmosphere. In contrast, Pierre Connes (Institut d'Optique, Orsay) and his team had been very successful in building a Fourier Transform interferometer for measuring the near-infrared spectrum of all bright planets (Connes et al. 1969) with a spectral resolution of 0.25 cm^{-1} (corresponding to a resolving power R higher than 15000). This may have influenced the choice that Michel Combes made to build a Fourier Transform interferometer to observe Jupiter in the 10-μm atmospheric window, previously observed by Gillett et al. (1969) at low resolution (Figure 1). The instrument built at Paris Observatory, however, was much less ambitious than the one built by Connes et al. (1969), as its highest spectral resolving power was only about 1000. The spectrum of Jupiter (Figure 2) between 10 and 13 μm was recorded with this instrument at the 2.2-m telescope of the University of Hawaii in 1977. It allowed the observation of stratospheric C_2H_2 and C_2H_6 - already detected by Ridgway et al (1976) - in emission, as well as tropospheric NH_3 and $^{15}NH_3$ in absorption. Figure 2 also shows, for comparison, the same spectrum of Jupiter as observed by ISO (also shown in Figure 1 with a different scale). The advantage of ISO was, of course, to cover the entire infrared range, as will be discussed below (Section 2.3). Using the 8-9 μm part of the spectrum, we were able to set constraints on the D/H ratio, in agreement with our estimate derived from HD/CH_4 (Encrenaz et al. 1980).

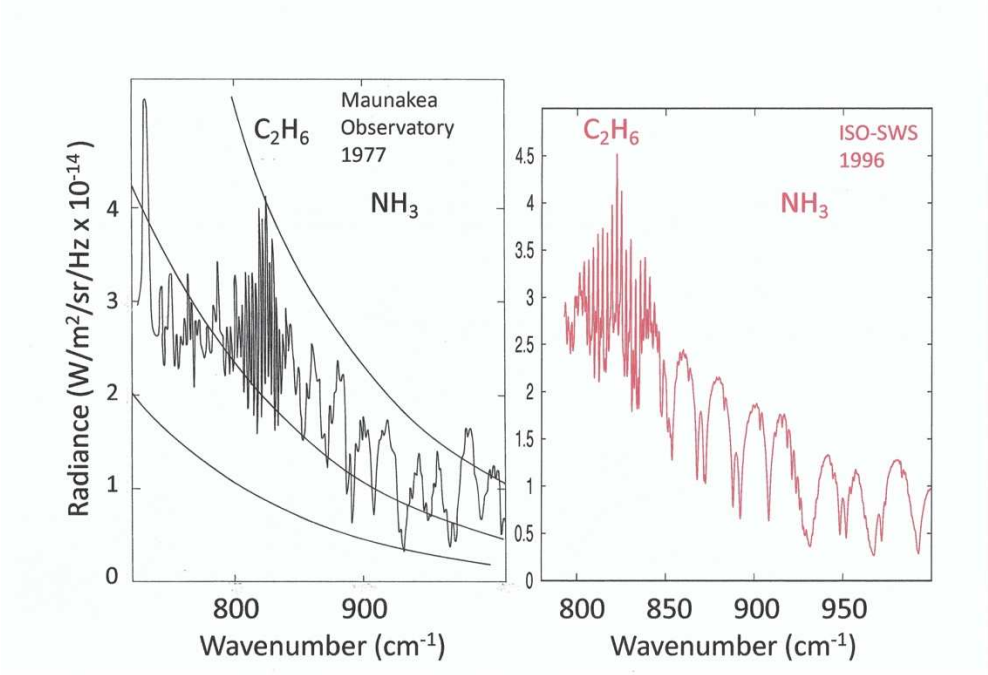

Figure 2. *Left: the spectrum of Jupiter, recorded between 10 and 13 μm at Maunakea Observatory, using a Fourier Transform interferometer (Encrenaz et al. 1978). Right: the spectrum of Jupiter in the same spectral range, recorded by ISO-SWS (Data from Encrenaz et al. 1996).*

The spectra shown in Figures 1 and 2 were acquired with single detectors which recorded the whole disk of Jupiter, or (in the case of ISO-SWS) the central part of the disk. Starting in the 1990s, spectral mapping became possible with the use of detector arrays, and later with bi-dimensional detectors. Some were used on ground-based facilities, like the 3.5-m New Technology Telescope (NTT) at the European Southern Observatory (ESO: www.eso.org) in La Silla, Chile; some others were flown on space missions, like NIMS (Near Infrared Mapping Spectrometer) aboard the Galileo mission. These two means were used at the time of the collision of comet Shoemaker-Levy 9 with Jupiter in 1994; these observations are described hereafter.

2.2 The collision of Shoemaker-Levy 9 with Jupiter

Discovered in April 1993, the comet Shoemaker-Levy 9 immediately appeared to be an exceptional object, having disrupted during its previous close flyby of Jupiter in July 1992. The "ring of pearls", made of about twenty individual fragments (named, in chronological order, from A to W), was orbiting around Jupiter and its collision with the planet was foreseen in July 1994 (Chodas & Yeomans 1996). This discovery led to an exceptional observing campaign including many observatories, from ground and space, covering the whole spectral range, from high energies to radio wavelengths. The comet crashed in the atmosphere of Jupiter at the 44°S latitude, in a series of consecutive impacts which spread in longitude, as a result of Jupiter's rotation, between July 16 and July 23, 1994. This rare event provided us with a unique opportunity to monitor remotely in real time the behavior of a planetary atmosphere subjected to a major meteoritic impact (Noll et al. 1996).

2.2.1 Temperature monitoring at ESO/NTT

Our observing program used the NTT telescope at ESO (La Silla, Chile), equipped with a bi-dimensional detector operating in the near infrared. Our plan was to monitor the behavior of a transition of H_3^+, at 3.53 μm; this ion had been detected in the upper Jovian stratosphere a few years earlier (Drossart et al. 1989), and is a tracer of the physical conditions of this region. At the time of the H impact (1994 July 18, 19:25:53 UT), the weather was clear and we were ready for monitoring the line emission on the screen. Because of the geometry of the event, the crash was occurring on the hidden side of the planet, and ground-based observers had to wait for fifteen minutes for the impact site to appear at the limb and become visible. At the exact expected time, a strong sinusoidal signal appeared on the screen, about twenty times stronger than the H_3^+ emission (Figure 3); it faded slowly and disappeared after about 30 minutes. This unexpected signal was indeed from Jupiter: it came from the thermal emission of the CH_4 molecules at high J-levels, usually too faint to be detected. From the observations, the temperature of the emitting region could be monitored (from 750 K at the beginning to 300 K thirty minutes later; Encrenaz et al. 1995). In addition, enhanced H_3^+ emissions were observed at 44N and 44S latitude, similarly distributed in longitude, showing evidence for a northern counterpart of the impact phenomenon (Schulz et al. 1995). This story tells us that, in any case, we have to be prepared for the unexpected…

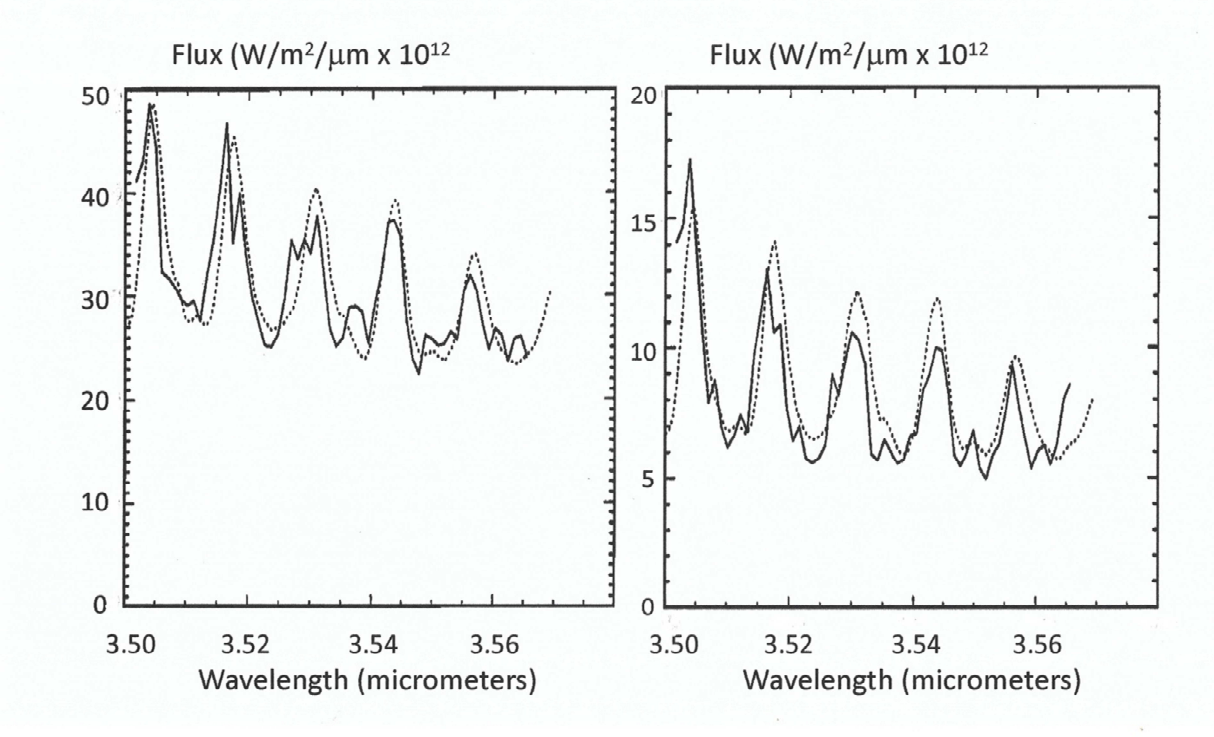

Figure 3. *Emission spectrum of methane around 3.53 μm at the time of the H impact. The ν_3 band peaks at 3.3 μm and its high-J components are usually not observed in the spectrum of Jupiter. At the time of the H impact, the temperature increased enough for these components to be observable. Monitoring them with time gives us a record of the temperature decrease in the Jovian stratosphere after the H impact. Left: first spectrum observed (solid line) compared with a model (dashed line; T = 750 K, P = 0.01 mb); right: spectrum observed 6 minutes later (solid line) compared with a model (T = 640 K, P = 0.01 mb). Source: Encrenaz et al. 1995.*

2.2.2 Water monitoring with Galileo/NIMS

At the time of the SL9 collision, the Galileo probe (www.jpl.nasa.gov/missions/galileo) was on its way to Jupiter. It was in a unique position to observe the crash, as its instruments were in direct view of the impact. Aboard Galileo, NIMS was an imaging spectrometer operating between 0.7 and 5.2 µm. In the fixed grating mode used for the SL9 observations, measurements are recorded simultaneously at 17 fixed wavelengths (Carlson et al. 1995). Data of the impact were limited to the 1.8 – 4.4 µm range, due to contamination by the reflected solar light and the thermal emission outside this spectral range. Most of the Jovian disk was included in the NIMS pixel.

Observations took place at the time of the splash phases following the G and R impacts, between 400 and 600 seconds after the fireball event (Encrenaz et al. 1997). In spite of the discrete wavelength sampling, emissions due to water and methane were easily identified, around 2.7 and 3.3 µm respectively. The CH_4 emission was used to infer the temperature evolution of the sequence, and the water content was inferred from the 2.7-µm emission. Figure 4 summarizes the results for the G and R events. In both cases, a maximum temperature of 1000 K was inferred, nine minutes after the fireball event, at pressure levels of 15 µbar and 10 µbar for G and R respectively. The inferred H_2O mass was (0.6 – 2.9) 10^{12} g for the G impact, and about ten times less for the R impact; these results were found in agreement with KAO measurements obtained at 6.2 and 7.7 µm (Sprague et al. 1996). The data also show that the water formation started in the splash phase, about 7 and 9 minutes after the explosion, for G and R respectively; it is also interesting to see that no carbon dioxide was detected. This observation would not have been possible from ground-based telescopes.

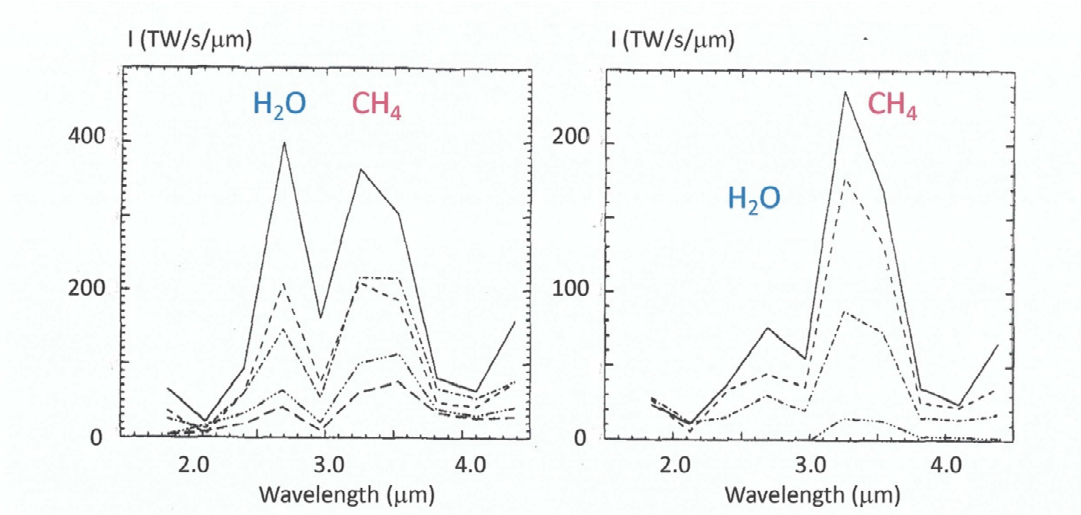

Figure 4. *Time sequence of the NIMS spectra during the splash phase following the G impact (left) and the R impact (right) at the time of the SL9 collision with Jupiter. The NIMS scans are summed over 1-minute intervals between 6 and 10 minutes after the fireball. The signal is increasing with time from bottom to top. Source: Encrenaz et al. 1997.*

The abundance of water inferred from our measurements has to be compared with the one of CO, the most abundant molecule, which was monitored in the millimeter range (2.5 10^{14} g, Lellouch et al. 1995). The relatively low water content suggests that the penetration level of

the impactors was above the tropospheric water cloud of Jupiter. The diameter of the comet, before its fractionation, was estimated to be about two kilometers (Solem, 1995).

Many other new species were discovered at the level of $10^{11} – 10^{12}$ g, in particular HCN which remained visible for many years. In 1996, it appeared that it was also the case of H_2O, which was detected in the stratosphere of Jupiter by the ISO satellite (see below, Section 2.3).

2.3 The giant planets as seen by ISO

The Infrared Space Observatory (ISO: www.cosmos.esa.int/web/iso) was a European satellite, launched by the European Space Agency (ESA: www.esa.int) in 1995, in operation until 1998. It consisted of a helium-cooled 60-cm telescope and four infrared instruments (a camera, a photometer and two spectrometers). It was designed for the study of the cold Universe, in particular the interstellar medium and protoplanetary disks. As a Mission Scientist aboard this mission, I had the opportunity of coordinating a solar system observing program which was especially fruitful in the case of giant planets and comets, in particular thanks to the Short Wavelength Spectrometer (SWS), whose Principal Investigator was Thijs de Graauw (SRON, Netherlands; de Graauw et al. 1996).

Figure 5 shows the spectra of Jupiter, Saturn and Neptune, as seen by ISO, between 2.3 and 16 μm (Encrenaz et al. 2003). The reflected component prevails below 4 μm, and the thermal emission dominates around 5 μm and above 6 μm. In the case of Saturn, the 5-μm emission is a mixture of reflected sunlight and thermal emission.

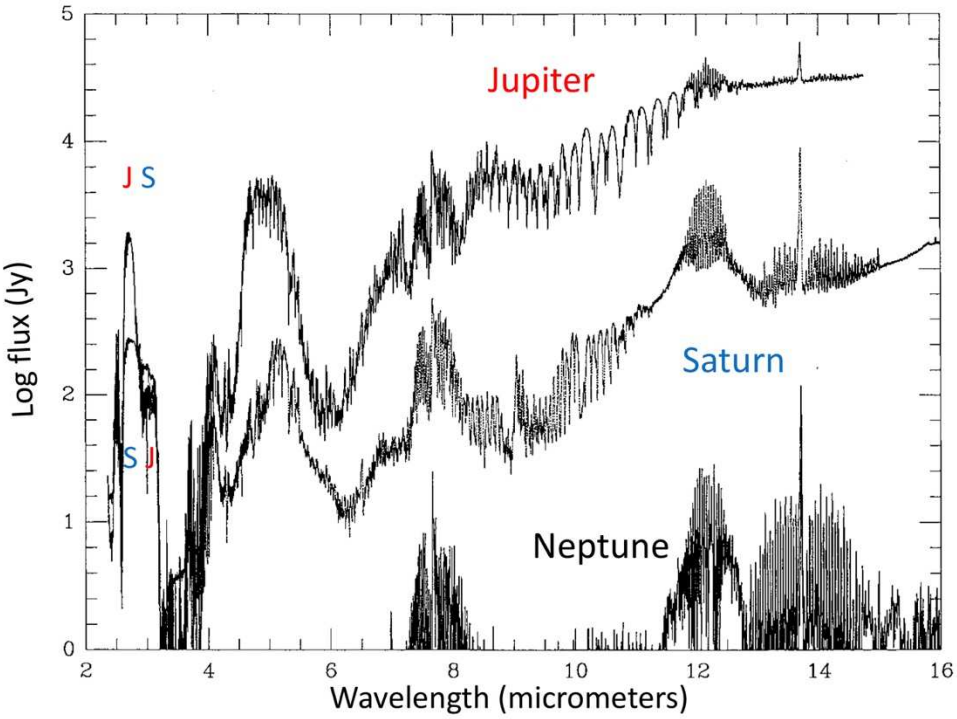

Figure 5. *The spectra of Jupiter, Saturn and Neptune (log scale) between 2 and 16 μm, as observed by ISO-SWS. The spectra of Saturn and Neptune are disk-integrated, while the Jupiter spectrum covers the central part of the disk. The spectrum of Uranus is not shown; it would appear only in the C_2H_2 band at 13.7 μm, with an intensity equal to a third of the Neptune value. Source: Encrenaz et al. (2003a).*

Regarding the giant planets, the main discoveries of ISO were the evidence for an external source of oxygen, and the measurement of deuterated hydrogen HD. In addition, new minor species were detected: C_3H_4 and C_4H_2 in Jupiter (Fouchet et al. 2000) and Saturn (de Graauw et al. 1997) with SWS, CH_3 in Saturn (Bézard et al. 1998) and Neptune (Bézard et al. 1999), and C_6H_6 outside the auroral regions of Jupiter and Saturn (Bézard et al. 2001). C_2H_4 was detected on Neptune, with the ISOPHOT instrument (Schulz et al. 1999). ISO also allowed for significantly improved constraints on the abundances of all the hydrocarbon photochemical products on the giant planets, including information on their vertical distributions (e.g. C_2H_2, see Moses et al. 2000a, 2005).

2.3.1 An external oxygen source in the stratospheres of the giant planets

In spite of the detection of water in Jupiter's stratosphere at the time of the SL9 collision, nobody expected to detect this molecule two years later. ISO detected H_2O in Jupiter, but also in the stratospheres of the other giant planets and Titan (Feuchtgruber et al. 1997; Coustenis et al. 1998; Figure 6). Several transitions appeared in emission between 20 and 40 μm, corresponding, within a factor of 10, to mixing ratios in the range of a few 10^{-9}. In addition, CO_2 was detected at 15 μm – also by ISO-SWS – on Jupiter, Saturn and Neptune (de Graauw et al. 1997; Bézard, 2000; Lellouch et al. 2002), confirming the existence of an oxygen reservoir in the stratospheres of these planets. Because of the presence of the tropopause which acts, for all objects, as a cold trap for H_2O, the origin of this reservoir had to be external. Two origins were proposed: (1) an interplanetary flux of meteoritic particles, as comets or smaller debris (Moses et al. 2000b) and (2) a contribution coming from the rings and satellites. In the case of Jupiter, a subsequent map obtained with the PACS imaging spectrometer of the Herschel submillimeter satellite has shown that the SL9 collision was indeed responsible for the distribution of stratospheric water as a function of latitude (Cavalié et al. 2013). What could be the origin of H_2O in the other giant planets? In the case of Saturn, one would expect the influence of rings and satellites to be more important, while the cometary source could prevail on Uranus and Neptune.

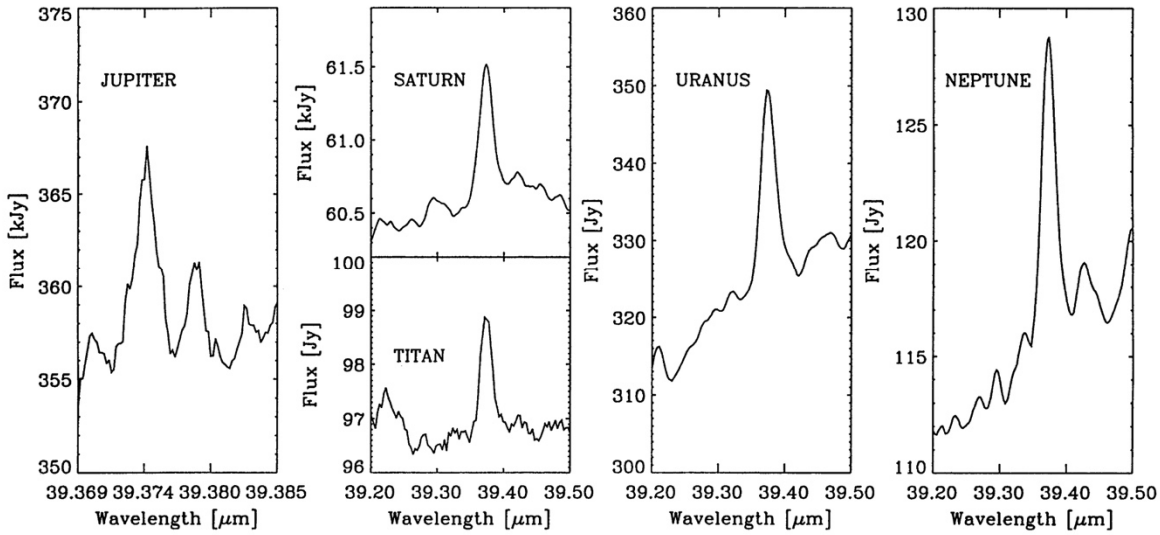

Figure 6. *Detection of the H_2O emission line at 39.4 μm on the four giant planets and Titan. In the case of Jupiter, the observation was made using the Fabry-Perot mode of SWS, with a spectral resolving power of 31000; in all other cases, the grating mode was used (R = 2000). Source: Feuchtgruber et al. (1999).*

2.3.2 Deuterium in the giant planets

Before the launch of ISO, it was not possible to obtain a measurement of D/H in the four giant planets using a single instrumental method. This became possible with ISO, using the R2 and R3 transitions of HD, at 37.7 μm and 28.5 μm respectively. From these transitions, D/H ratios of 2.25 +/- 0.35 x 10^{-5} and 1.7 (+0.75, -0.45) x 10^{-5} were retrieved for Jupiter and Saturn respectively (Lellouch et al. 2001), and values of 5.5 x 10^{-5} and 6.5 x 10^{-5} were inferred for Uranus and Neptune respectively (Feuchtgruber et al. 1999). The values of Uranus and Neptune were later reduced to 4.4 +/- 0.4 x 10^{-5} and 4.1 +/- 0.4 x 10^{-5}, using the R1 HD line at 56 μm with the PACS instrument aboard the Herschel submillimeter satellite (Feuchtgruber et al 2013).

Two comments can be made about these results. First, the D/H ratio in Saturn seems to be slightly lower than the Jupiter value, which is not expected by the models, since the mass fraction of the initial core, in the case of Saturn, is expected to be larger than in the case of Jupiter. We have presently no explanation for this discrepancy. The second comment is that D/H in the giant planets follows the trend expected in the case of the core-accretion model, with larger values in Uranus and Neptune, as compared with Jupiter and Saturn. This measurement, as the one of C/H in the four giants, comes as a support to the core-accretion model of the giant planets (Owen and Encrenaz 2006).

2.4 Uranus

As shown in Figure 5, the 5-μm region, free of methane absorption, is an atmospheric window where the deep troposphere of Jupiter and Saturn can be probed. In the case of Jupiter, the

radiation is fully of thermal origin while, in the case of Saturn, there is a significant contribution of solar reflected radiation. In the case of Uranus and Neptune, this atmospheric window should be fully of solar reflected origin, since the temperature of the probed region is expected to be around 120 K, and the blackbody radiation corresponding to such a low temperature is too weak to be detectable. As shown in Figure 5, ISO was not able to detect this component in Uranus nor in Neptune, so, in 2000, we began an observing program at IRTF, using the SpeX imaging spectrometer at the IRTF (Rayner et al. 2003). Our objective was to search for tropospheric CO and (possibly) PH_3 in Uranus (easier to observe than Neptune); both species were expected to be in absorption, as in the case of the two other giant planets, and their detection would bring an important diagnostic for constraining the planet's origin and evolution.

Our observations led to a surprise. We did not detect the continuum at 4.5 μm, but, instead, we observed a set of H_3^+ emission lines, between 3.5 and 4.7 μm. The H_3^+ ion had been discovered in Jupiter ten years earlier (Drossart et al. 1990), and later on Saturn and Uranus (Trafton et al. 1993), so it was not a new discovery, but this observation allowed us to infer the rotational temperature of the emitting region, in the upper stratosphere, and an estimate of the H_3^+ abundance in Uranus. Combined with other data, our results are consistent with a correlation between the H_3^+ emission and the solar radiation, modulated by the solar cycle (Encrenaz et al. 2003b). However, the 4.5-μm continuum signal was too weak to be analyzed. In 2003, we used a more sensitive instrument, the ISAAC imaging spectrometer at the Very Large Telescope. Again, the result was surprising. The weak continuum at 4.5 μm was indeed detected, but the spectrum appeared to be dominated by a series of CO fluorescence lines (Encrenaz et al. 2004a; Figure 7). Such a fluorescence phenomenon is not common in giant planets' atmospheres; it has been observed only in CH_4 emission lines at 3.3 μm in the case of Jupiter and Saturn, at high stratospheric levels (Drossart et al. 1999). From this observation, a mixing ratio of 3 x 10^{-8} was tentatively inferred in the stratosphere of Uranus. From the absence of CO and PH_3 features in the weak continuum, upper limits of 2 x 10^{-8} and 10^{-6} were respectively derived for the tropospheric mixing ratios of these species, suggesting an external origin for the stratospheric CO. The detection of CO was later confirmed with the Herschel submillimeter satellite, but the CO abundance was found to be about 8 x 10^{-9}, i.e. significantly lower than the earlier estimate (Teanby and Irwin, 2013; Cavalié et al; 2014).

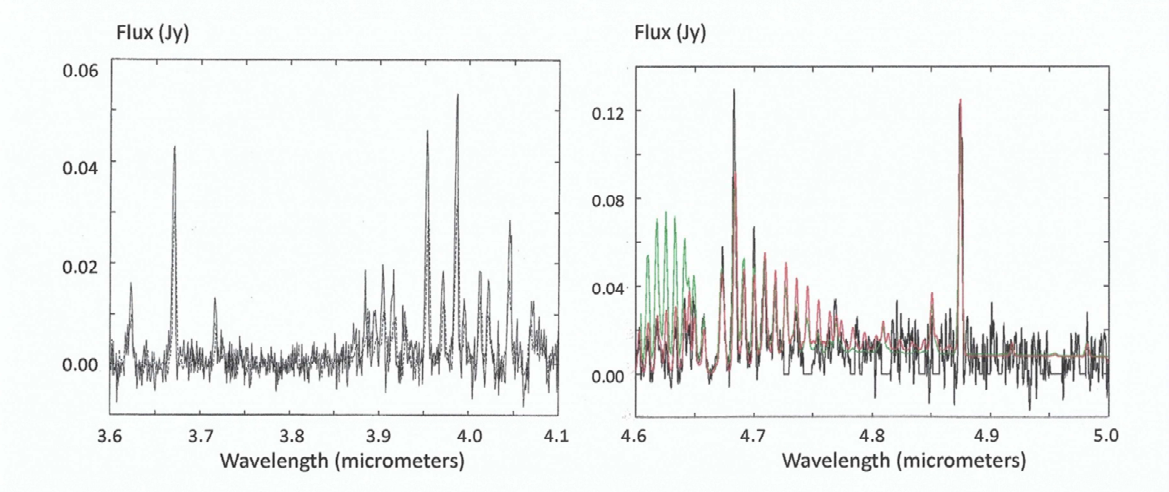

Figure 7. *Left: The spectrum of Uranus between 3.6 and 4.1 μm, observed with SpeX at IRTF (Maunakea Observatories). All emission lines are due to H_3^+. Solid line: September 2000; dashed line: September 2001. The inferred rotational temperature is 560 K in 2000, and 640 K in 2001. Source: Encrenaz et al. (2003b). Right: the spectrum of Uranus (black line) recorded with ISAAC at the VLT (ESO, Paranal) between 4.6 and 5.0 μm. H_3^+ emission lines are present at 4.67 and 4.87 μm. CO emission appears between 4.6 and 4.8 μm. Red line: best fit model including CO fluorescence. Green line: model including CO thermal emission. Source: Encrenaz et al. (2004a)*.

2.5 Neptune

Although SpeX at the IRTF and ISAAC at the VLT were using bi-dimensional detectors, our observations of Uranus were not spatially resolved and integrated most of the planetary disk. A few years later, another imaging spectrophotometer, also at the VLT, allowed us to obtain the first thermal images of Uranus and Neptune.

In September 2006, we used VISIR (VLT Imager and Spectrometer for mid Infrared; Lagage et al. 2004) in the imaging mode to map the disks of Uranus and Neptune in different filters to probe different atmospheric levels. In particular, the 18.7 μm filter probes the tropopause where the temperature is minimum. At this wavelength, the spectrum is dominated by hydrogen collision-induced absorption; since H_2 is uniformly distributed over the planet, a map at 18.7 μm shows the temperature distribution at the tropopause. The result was very surprising (Figure 8). While the map of Uranus showed moderate variations as a function of latitude (Orton et al. 2009), the map of Neptune exhibited a strong maximum near the south pole, corresponding to a maximum temperature of 62 K, 7 K above the disk-averaged temperature (Orton et al. 2007). This temperature increase has been tentatively interpreted as the consequence of the maximum solar irradiation received at the south pole over several decades, as southern solstice occurred in July 2005. A consequence of this anomaly is the release of methane, elsewhere cold-trapped in the troposphere, to escape in the stratosphere; this result provides us with an explanation for the high abundances of stratospheric methane reported previously (Baines & Hammel 1994; Baines et al. 1995), significantly higher than those corresponding to the saturation vapor pressure at the average minimum temperature (55 K). Another possible explanation is adiabatic heating from downwelling or other dynamical phenomena (Karkoschka and Tomasko, 2011; de Pater et al. 2014; Lellouch et al. 2015).

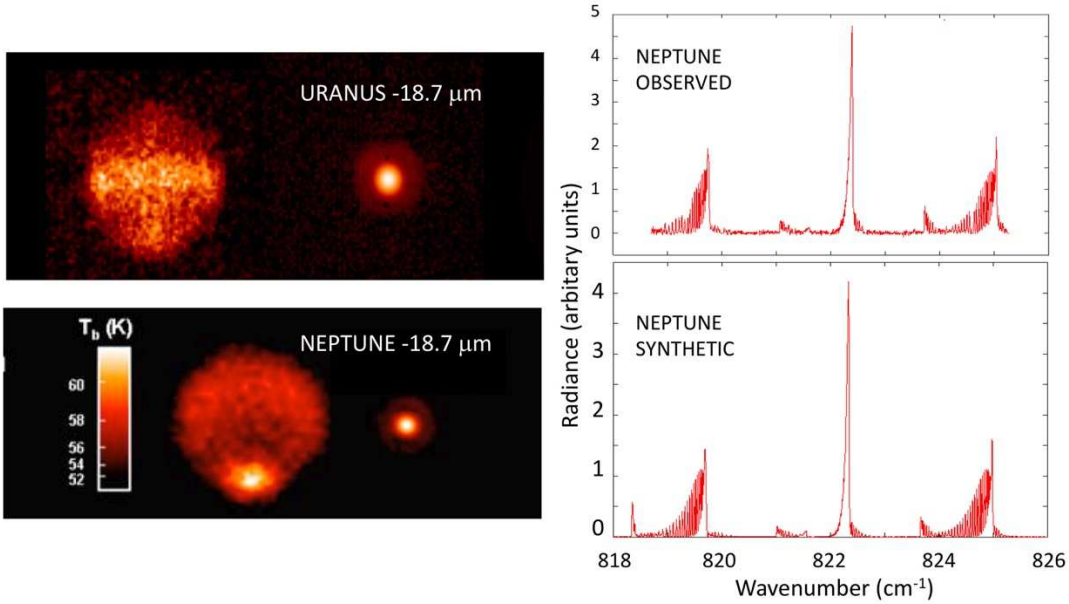

Figure 8. *Left: images of Uranus (top) and Neptune (bottom) recorded at 18.7 µm with VISIR at the VLT (ESO, Paranal) in September 2006. In both cases, the north pole is at the top of the figure. Source: Orton et al. (2007, 2015). Right: the disk-integrated spectrum of Neptune, recorded with the TEXES imaging spectrometer at IRTF (Maunakea Observatories) in June 2003, with a spectral resolving power of 80000. Top: the observed spectrum; bottom: the synthetic spectrum. Source: personal archives.*

In the early 2000s, another thermal imaging spectrometer became available. TEXES (Texas Echelon Cross-Echelle Spectrograph), designed and built by John Lacy (University of Texas), and operated by John Lacy, Matt Richter and Tommy Greathouse, was mounted at the IRTF (Lacy et al. 2002). This instrument, operating between 5 and 25 µm, combines imaging capabilities with different spectroscopic modes, including a high spectral resolution mode (R > 80000). With such a high resolving power, this instrument appeared to be perfectly suited for planetary mapping of minor atmospheric species. In the case of Neptune, we used TEXES in 2003 to observe the stratospheric emission band of ethane (C_2H_2). Figure 8 (right) shows the disk-integrated spectrum of Neptune and illustrates the exceptional quality of the data. These data also provided us with the resolved spectrum of acetylene C_2H_4 on Neptune. In 2007, TEXES was used at the 8-m GEMINI telescope, also at the Maunakea Observatories, to map the disk of Neptune and to retrieve information on the distribution of temperature and various hydrocarbons (Greathouse et al. 2011).

3. Terrestrial planets

It is well established that the atmospheres of the terrestrial planets – Venus, the Earth, and Mars – exhibit, at their surfaces, extremely different conditions. At 0.7 au from the Sun, the surface pressure of Venus (93 bars) is almost a hundred times the terrestrial value, and its temperature is close to 730 K; in contrast, on the other side of the Earth, at 1.52 au from the Sun, the surface pressure of Mars, averaged over the season, is less than one hundredth of a bar, and its mean temperature is around 220 K. What is less well known are the reasons for

such extreme conditions. It is generally believed that the three planets were formed in a common environment, relatively close to the Sun, from the accretion of solid refractory particles that led to the formation of dense, rocky planets. This scenario, known as the core accretion model of planetary formation, is also supported by the fact that both Venus and Mars have a CO_2-dominated atmosphere with a few percent of N_2, which was also probably the case of the primordial atmosphere of the Earth. The presence of massive amounts of water on Earth today suggests that, originally, water was equally present on Venus and Mars, at their surface and in their atmospheres; indeed, we find signatures of past water on both planets, especially through the D/H ratio, as will be discussed below. Why and how did the three planets evolve, from relatively comparable initial conditions, to the diverging conditions that we observe today? Answering this question is a major challenge in today's planetary research.

In this section, I will present observations of Mars and Venus that have been performed from the ground over the past two decades, using the TEXES instrument at IRTF (Maunakea Observatories). As described above (Section 2.4), TEXES is an imaging spectrometer operating in the thermal range, which allows us to obtain instantaneous maps of minor species over planetary disks. Thanks to the high resolving power of TEXES (up to 80000), it is possible to monitor trace species with vertical mixing ratios in the range of a few ppbs, and to follow their day/night, latitudinal or seasonal variations, as well as transient phenomena. These observations can provide a precious complement to in-orbit space observations, which are often limited to specific local times and restricted planetary areas.

In the next sub-sections, I will describe long-term observing campaigns that have been performed to monitor the seasonal behavior of hydrogen peroxide and water vapor on Mars (Section 3.1) and to study the sulfur and water cycles on Venus (Section 3.2). In addition, TEXES observations have been used to derive upper limits of SO_2 on Mars (Encrenaz et al. 2011) and PH_3 on Venus (Encrenaz et al. 2020a).

3.1 Mars

With its very tenuous atmosphere, Mars has a "simple" spectrum, fully dominated by CO_2, both in its reflected sunlight and its thermal emission. Weak signatures of water vapor and carbon monoxide are also present. Until 2004, the only other identified trace component was ozone O_3. For over two decades, the climate of Mars has been successfully modelled through the use of Global Climate Models (GCMs) derived from those developed for the terrestrial climate (Forget et al. 1999). Generally speaking, these models provide a good fit of the observations, illustrating that the main mechanisms (circulation, condensation, photochemistry) are globally well understood.

Still, there are pending open questions. One of them raised after the Viking exploration: what was the oxidant responsible for the destruction of organics at the surface of Mars? Hydrogen peroxide (H_2O_2) was soon suspected, as its presence was predicted by photochemical models, and was searched for repeatedly until Todd Clancy and his team identified it in the submillimeter range (Clancy et al. 2004). In parallel, using TEXES at IRTF, we have searched for H_2O_2, finally detected it, and mapped it on Mars to monitor its seasonal behavior (see below, Section 3.1.1). Another pending question was the water cycle on Mars today, and, even more

important for understanding the water evolution, the water content of the early Mars. Both questions are addressed below (Sections 3.1.2 and 3.1.3).

3.1.1 Hydrogen peroxide mapping and seasonal behavior

At the time of the Viking exploration, the negative results of the biological experiments suggested the presence of a powerful oxidizer, and hydrogen peroxide (H_2O_2) was suggested as a possible candidate (Oyama and Berdahl 1977). The presence of small amounts of H_2O_2 (less than 100 ppbv) was actually expected on the basis of photochemical models (Atreya and Gu 1994; Nair et al. 1994; Krasnopolsky 1995). After unsuccessful attempts (Krasnopolsky et al 1997, Encrenaz et al. 2002), the detection of H_2O_2 on Mars was first announced by Clancy et al. (2004), using the JCMT sub-millimeter telescope at Maunakea Observatories). In parallel we searched again for H_2O_2 and were able to detect and map the molecule (Encrenaz et al. 2004b), using the TEXES imaging spectrometer at IRTF.

As mentioned above (Section 2.4), TEXES has the advantage of combining a high spectral resolving power and very good imaging capabilities, which makes it a perfect tool for mapping minor atmospheric species. We selected the H_2O_2 ν_6 band centered at 1266 cm^{-1} (7.9 μm), in a region relatively free from telluric contamination, and we chose a small spectral interval, free of telluric absorption, where weak neighboring transitions of both H_2O_2 and CO_2 are present. In order to estimate the H_2O_2 mixing ratio over the Martian disk, we simply ratio the H_2O_2 line depth by the CO_2 line depth. This first-order method (actually derived from our earlier analyses: Combes and Encrenaz 1979) has the advantage of minimizing the uncertainties associated with surface and atmospheric properties, including thermal profile, dust opacity and airmass factor. This procedure best applies in the case of optically thin lines, but can also be used if the depths of the lines (convolved at the TEXES spectral resolution) are less than a few percent. Indeed, synthetic calculations have shown that in this case, within a few percent, the H_2O_2 mixing ratio varies linearly with the H_2O_2/CO_2 line depth ratio, over a wide range of atmospheric parameters (Encrenaz et al. 2008).

We started searching for H_2O_2 in February 2001, when Mars was near northern summer solstice (Ls = 112°). This situation looked favorable as it corresponds to a maximum of water vapor near the north pole and, according to photochemical models, H_2O and H_2O_2 are expected to be correlated. Surprisingly, H_2O_2 was not detected and the inferred upper limit (6 ppbv) was difficult to reconcile with the models (Encrenaz et al. 2002). Two years later, we detected H_2O_2 with a maximum mixing ratio of 40 ppbv (Encrenaz et al. 2004). Then, we regularly monitored the H_2O_2 distribution as a function of latitude and season until 2019. Figure 9 shows an example of the spectrum used to infer the H_2O_2 mixing ratio and two examples of maps corresponding to different seasons, compared with GCM models (Forget et al. 1999). In both cases, the agreement is satisfactory.

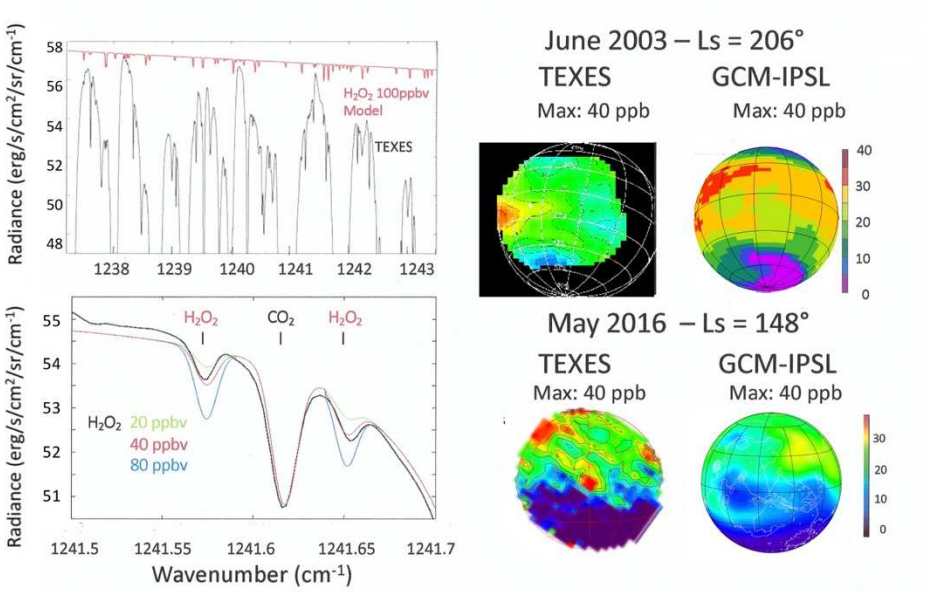

Figure 9. *Left panel, top: the TEXES spectrum (black) recorded in the region of maximum H_2O_2 on June 2003. A model of H_2O_2 absorption is shown for a mixing ratio of 100 ppbv. Left, bottom: an enlargement showing the H_2O_2 and CO_2 lines used to derive the map. Right panel, top: the TEXES map corresponding to the spectrum shown on the left (June 2003), compared with a GCM-IPSL model. Source: Encrenaz et al. (2004). Note that the absolute value of the H_2O_2 vmr was rescaled after 2015 (see text and Figure 10). Right, bottom: a H_2O_2 map obtained for another season (May 2016, Ls = 148°). Source: Encrenaz et al. (2019a).*

Figure 10 shows the seasonal variations of H_2O_2 recorded between 2001 and 2019. Most of the data are from TEXES, with the exception of two sub-millimeter measurements, the first detection by Clancy et al. (2004) for Ls = 250°, and an upper limit by Hartogh et al. (2010) with the Herschel space observatory (www.esa.int/Science_Exploration/Space_Science/Herschel) for Ls = 77°. In 2015, a problem arose when it was realized that the H_2O_2 spectroscopic intensities used before, taken from the GEISA-2003 database, were lower than the GEISA-2015 database by a factor close to 2. As a result, all TEXES values published prior to 2015 (open squares in Figure 10) had to be recalibrated (black and green squares). The data were compared to different models, involving homogeneous chemistry (Lefèvre et al. 2008, Daerden et al. 2018), and heterogeneous chemistry on water ice particles (Lefèvre et al. 2008). Our first conclusion (Encrenaz et al. 2012a) was that the comparison between the data and the models favored heterogeneous chemistry; however, the recalibration of the H_2O_2 data showed that there is a discrepancy between the data and the models: in most of the cases, the measurements are lower than expected by a factor close to 2, whichever homogeneous or heterogeneous chemistry is considered. We have presently no explanation for this discrepancy.

Another surprising result is shown in Figure 10. For several values of the solar longitude (Ls around 80°, 100°, 150° and 207°), the H_2O_2 abundances show different values, depending on the Martian year. In the last case, a possible explanation is that the upper limit of H_2O_2 was obtained in July 2018, at the time of the global dust storm. Models developed by Daerden et al. (2018) were able to account for the absence of H_2O_2 under these conditions (Encrenaz et

al. 2019a). But, in the three other cases, we have no explanation for the observed interannual variations.

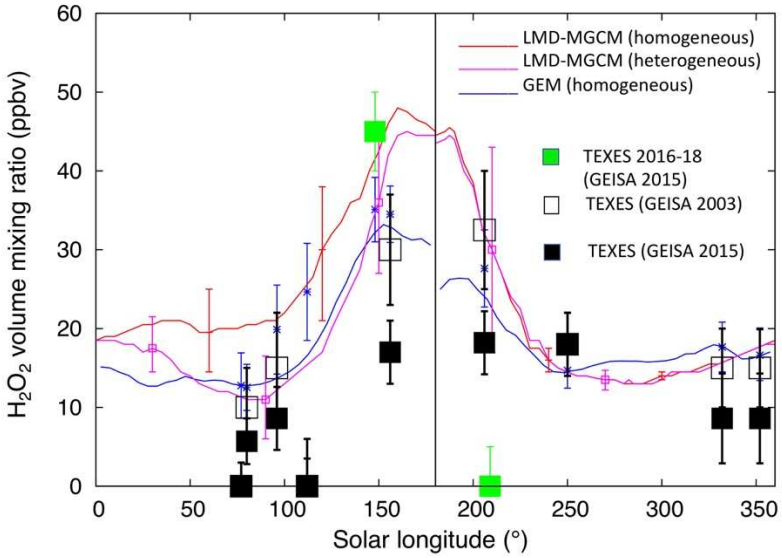

Figure 10. *Seasonal variations of the H_2O_2 mixing ratio as a function of the solar longitude Ls. Open squares: TEXES data prior to 2015 (using the GEISA-2003 database); black squares: final dataset, including the TEXES recalibrated data and the two sub-millimeter measurements at 77° by Hartogh et al. (2010) and 250° by Clancy et al. (2004). Green squares: TEXES data from 2016 and 2018. The 2018 upper limit corresponds to the global dust storm; other discrepancies are unexplained. Models: GCM-IPSL, with homogeneous chemistry (red) and heterogeneous chemistry (purple), by Lefèvre et al. (2008); GEM model with homogeneous chemistry (blue) by Daerden et al. (2019). Source: Encrenaz et al. (2019a).*

In summary, our analysis of the behavior of hydrogen peroxide on Mars reveals that its observed abundances are below the predictions. This discrepancy might suggest the possible presence of another oxidizer, still to be identified, or could be due to another loss process for H_2O_2, not taken into account in the current photochemical models.

3.1.2 Water vapor on Mars

In June 2003, as we were searching for H_2O_2 around 8 µm, we realized that a few weak HDO transitions were present in the spectral interval that we had selected for H_2O_2 (1227–1243 cm^{-1}). We took advantage of these transitions to obtain water vapor maps, simultaneously with H_2O_2 maps. It was possible to use HDO as a proxy for H_2O, because, as shown by Montmessin et al. (2005), the variations of H_2O over the Martian disk are expected to be much stronger than the variations of D/H (derived from the HDO/H_2O ratio). Indeed, the water seasonal cycle of Mars has been well known since the Viking experiments (Jakosky and Farmer 1982) and later with the TES instrument aboard the Mars Global Surveyor orbiter (Smith 2002, 2004). Water vapor was found to exhibit a strong maximum at high northern latitudes around the northern summer solstice, and a weaker maximum at the south pole near southern summer solstice, with latitudinal variations by a factor as high as 10. The D/H ratio in the Martian atmosphere was found to be enriched by a factor 5–6 with respect to the VSMOW (Vienna

Standard Mean Ocean Water, i.e. 1.56 x 10^{-4}) terrestrial value (Owen et al. 1988, Krasnopolsky et al. 1997; see Section 3.1.3), and no large variations over the disk were expected (Fouchet and Lellouch 2000); this was later confirmed by more sophisticated models, showing that seasonal variations of D/H are expected to be less than 10 - 15% for latitudes between 60°N and 60°S (Montmessin et al. 2005).

Figure 11 shows examples of water vapor maps obtained using the line depth ratio method described above. The first example corresponds to the same dataset as shown in Figure 10 (top right). We used a HDO transition at 1240.0 cm^{-1}, very close to the H_2O_2 doublet shown in Figure 10, and we used the CO_2 line at 1241.6 cm^{-1} (already used for the H_2O_2/CO_2 line depth ratio) for comparison. The second example is extracted from the May 2008 dataset; in this case, we used another HDO transition at 1236.3 cm^{-1}. In both cases, the observed H_2O maps were found to be in agreement with the GCM predictions (Forget et al. 1999), both for the absolute water vapor abundance and for the H_2O spatial distribution. In both cases, the water vapor content is maximum in the northern hemisphere, as expected during northern spring and early summer (Smith, 2002, 2004).

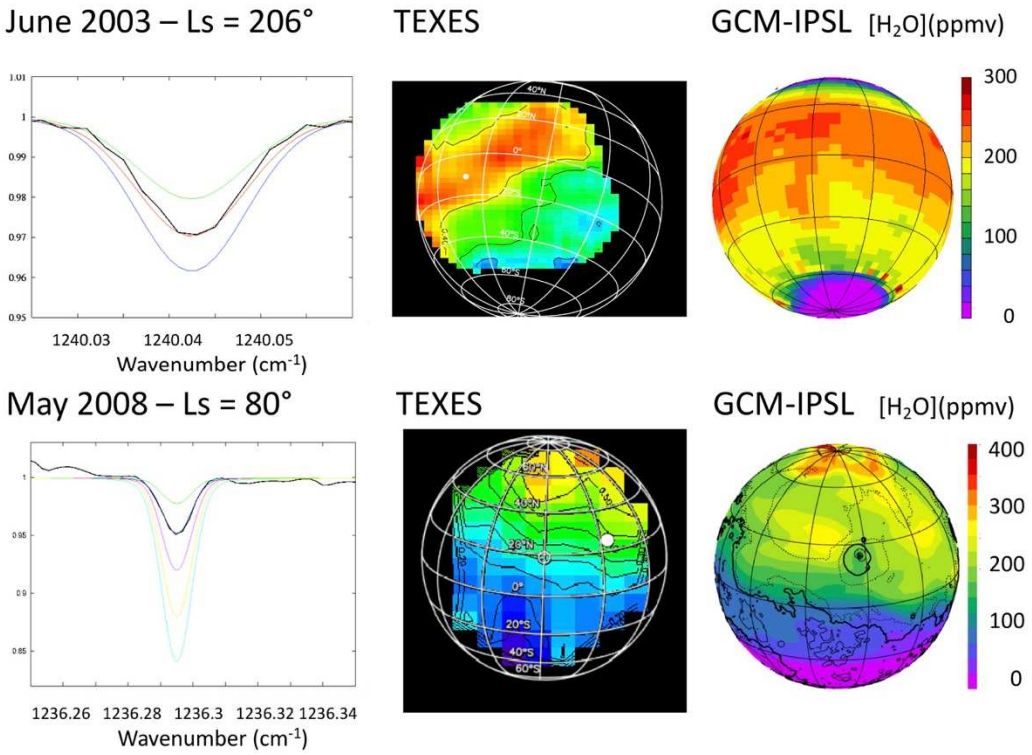

Figure 11. *Left: TEXES spectra (black) of two HDO transitions used to retrieve the water vapor maps shown on the middle of the figure. Top: Observations of June 2003 (Ls = 112°); the best fit is obtained for a H_2O mixing ratio of 300 ppmv (red curve; the green and blue curves correspond to 200 and 400 ppmv respectively). Bottom: Observations of May 2008 (Ls = 80°); the best fit is obtained for H_2O = 250 ppmv (blue curve; the green and red curves correspond to 100 and 500 ppmv respectively). Middle: HDO maps inferred from the spectra (top: June 2003; bottom: May 2008). The unit on the maps is the HDO/CO_2 line depth ratio. Right: GCM maps calculated for the conditions of the observations (top: June 2003; bottom: May 2008).*

The unit is the H_2O /CO_2 mixing ratio. Sources: Encrenaz et al. (2005) (top) and Encrenaz et al. (2010) (bottom).

3.1.3 D/H mapping on Mars with EXES on SOFIA

While the seasonal cycle of water vapor on Mars is well understood by the climate models, the very low abundance of water on Mars (as well as on Venus) today remains a puzzle. It is now generally accepted that, as in the case of the Earth, the water abundance in the primitive atmospheres of Mars and Venus was much higher than today; however, its abundance is poorly constrained presently. In the case of Mars, there are many signs (including channel incision, putative northern ocean, deuterium enrichment etc (see e.g. Catling and Kasting 2017), leading to estimates of the early water inventory between a hundred and a thousand meters of GEL (global equivalent layer).

The HDO/H_2O ratio on Mars is a diagnostic of the early water content of the planet, because, in the upper atmosphere, the H atoms escape more easily than the D atoms. Such a mechanism is especially efficient in the case of Venus, where a D/H enrichment by a factor 120 has been inferred from the study of HDO and H_2O in the lower atmosphere (Bézard et al. 1990). In the case of Mars, the enrichment (factor of about 5) is more modest, but still very significant for the very tenuous atmosphere of Mars. An early estimate of D/H (< 1.2 VSMOW) was derived from SNC meteorites (Usui et al. 2012, Hallis et al. 2012), and a D/H enrichment by a factor 3 was inferred by the Curiosity rover in ancient clays, dated from 3.5 Gy ago (Mahaffy et al. 2015). Still, the measurement of D/H on Mars has led to very different estimates of the early water reservoir (Krasnopolsky 2002, Villanueva et al. 2015), due to the uncertainty in the fractionation factor indicating the efficiency of D escape relative to H escape. Another uncertainty is the determination of the current D/H on Mars, globally averaged over latitudes, longitudes and seasons.

As a contribution to this study, we have set up an observing program to globally map the D/H ratio over the Martian disk and for different seasons. Another objective was to study the present water seasonal cycle through fractionation due to differential condensation processes. Indeed, deuterium is known to be enriched in the ice phase, through the so-called Vapor Pressure Isotopic Effect (VPIE; Merlivat & Lief, 1967). On Mars, the D/H ratio is expected to be maximum at the north pole at northern summer solstice, just after the content of the northern water ice cap is released in the atmosphere (Montmessin et al. 2005). Our objective was thus to test the VPIE mechanism.

In order to determine the Martian D/H ratio in water using our line depth ratio method, we needed to use weak neighboring transitions of HDO and H_2O. which requires that the observations take place above the terrestrial troposphere, so as to eliminate the terrestrial water vapor absorption lines. The EXES (Echelle Cross Echelon Spectrograph) aboard the Stratospheric Observatory for Infrared Astronomy (SOFIA: www.nasa.gov/mission_pages/SOFIA/overview/index.html), jointly developed by NASA and DLR, gave us this opportunity. EXES, under the PIship of Matt Richter (UC Davis, CA), is directly derived from TEXES, with a slightly enlarged spectral range (4.5 – 28.3 μm) and increased spectral resolving power (close to 10^5). Several flights occurred between 2014 (when EXES became operational) and 2018. Observations were performed around 1360 cm^{-1} (7.2 μm)

where weak transitions of HDO, H_2O and CO_2 occur. The advantage of the line depth ratio method is that it allows us to derive the HDO/H_2O directly, without using the CO_2 transitions, which removes uncertainties associated with the thermal structure. Still, we also used the CO_2 transition to infer the HDO and H_2O mixing ratios and to check they were in agreement with the GCMs (Encrenaz et al. 2016a, 2018, 2019b).

Figure 12 shows three maps of D/H obtained with EXES in 2014, 2016 and 2018 respectively. In all cases, the D/H maps appear to be remarkably uniform, with a disk-integrated D/H value between 4.0 and 4.4 times the (VSMOW) terrestrial value. The figure also shows an example of disk-integrated spectrum, taken in April 2014; the best fit corresponds to a D/H value of 4.4 (+ 1.0, - 0.6) x VSMOW. The values inferred from the two other maps are very similar. Our conclusion is thus that we see no significant change of the disk-integrated value of D/H over the two observed seasons (early northern summer and southern solstice), nor any strong variation of D/H over the Martian disk. Regarding the spatial distribution of D/H, however, we have to keep in mind that the spatial resolution of SOFIA (3 arcsec) is, unfortunately, very poor, so that our images are significantly blurred, as compared, for example, with those of Villanueva et al (2015). Another conclusion from our study is that the D/H variations over the Martian disk are in agreement with the predictions of the VPIE model (Montmessin et al. 2005), and our disk-integrated value of D/H is in agreement with the measurements by Krasnopolsky (2015).

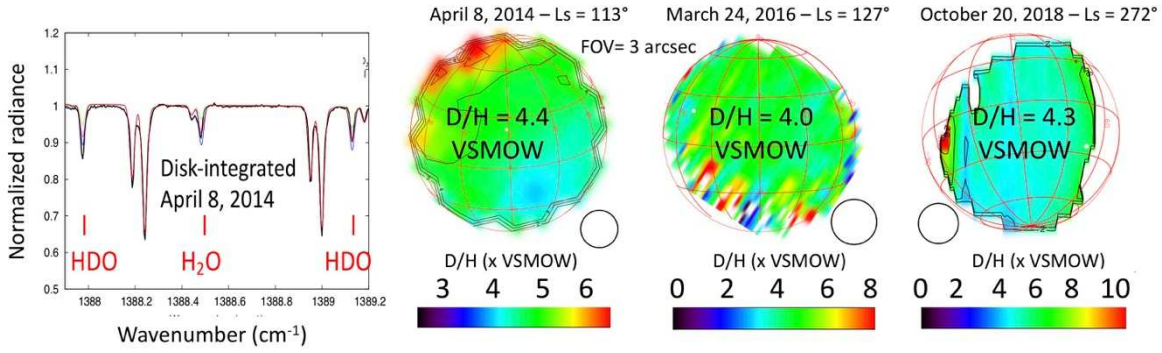

Figure 12. *Left panel: The EXES disk-integrated spectrum of Mars around 7.2 µm, recorded on April 8, 2014. Right panel: 3 maps of D/H obtained in 2014, 2016 and 2018. The disk-integrated D/H values are 4.4, 4.0 and 4.3 x VSMOW respectively. The minimum on the 2014 map corresponds to the Tharsis plateau, in agreement the VPIE model predictions (Montmessin et al. 2005) and with the observations by Villanueva et al. (2015). Sources: Encrenaz et al. 2016a, 2018, 2019b*

3.2 Venus

In spite of their common composition, dominated by carbon dioxide, the atmosphere of Venus is by far less well understood than the Martian atmosphere. While global climate models of Mars have been developed for over twenty years (Forget et al. 1999), GCMs of Venus are still in progress (Lebonnois et al. 2016, Gilli et al. 2021, Navarro et al. 2021), and consider separately the troposphere below the clouds and the mesosphere above. The chemistry of the Venus atmosphere is dominated by the cycles of sulfur and water. Both SO_2 and H_2O are abundant in the troposphere (150 ppmv and 30 ppmv respectively; Bézard & de Bergh 2007),

and they are transported above the main cloud deck by Hadley convection (Prinn & Fegley 1987). SO_2 is photodissociated above the clouds by the solar UV radiation and combines with H_2O to form H_2SO_4 which condenses to form the clouds (Zhang et al. 2010, 2012). At the cloud top and above the clouds, water is depleted by a factor of about 30 (Fedorova et al. 2008), while SO_2 is depleted by a factor of 300–1000 (with mixing ratios of 150-500 ppbv; Marcq et al. 2011, 2013; Belyaev et al. 2012); this factor is much larger than expected if SO_2 were only associated with H_2O to form H_2SO_4. Above the clouds, SO_2 continues to be depleted as the altitude increases, down to the level of a few ppbv. What happens to sulfur between the troposphere and the mesosphere? It is probably trapped in the clouds in the form of aerosols, still to be identified. But another surprise occurs in the upper mesosphere : submillimeter observations have shown that SO_2 is again present at the level of a few tens or hundreds of ppbv (Sandor et al. 2010), which implies the presence of another sulfur reservoir, which also remains to be identified.

There are other open questions related to the atmosphere and the surface of Venus (Taylor 2014). What is the origin of the long-term variations of the SO_2 abundance at the cloud top (Esposito, 2004; Marcq et al. 2013)? Is there active volcanism today, as suggested by infrared observations by Venus Express (Smrekar et al. 2010)? What is the origin of the super-rotation and what are the mechanisms of the atmospheric circulation? What are the coupling mechanisms between the troposphere and the mesosphere? These questions (and others) will be addressed by the future space missions toward Venus, Veritas, Envision and Da Vinci, in the next decade.

3.2.1 SO_2 and HDO mapping with TEXES

In the context of the successful exploration of Venus by the Venus Express mission, and then by the Akatsuki mission, we set up an observing program, using TEXES at IRTF, to monitor both SO_2 and H_2O at the cloud top in support of these missions. Indeed, both molecules have strong infrared transitions around 7 μm and can be simultaneously observed, together with CO_2. As in the case of Mars, the simultaneous observation of weak transitions of these three molecules is needed to estimate their mixing ratios.

Our observing campaign started in January 2012 and is still ongoing, after the interruption due to the Covid crisis in 2020. Most of the observations were recorded at 7.4 μm (where the cloud top is probed) and 19 μm (where the radiation comes from within the clouds, a few km below the cloud top). In addition, some observations were done at 8.6 μm where the radiation comes from a few km above the cloud top. Indeed, this wavelength corresponds to the maximum of the H_2SO_4 extinction coefficient, responsible for the infrared opacity of the cloud (Zasova et al. 1993). HDO (used as a proxy of H_2O, as in the case of Mars) is observed at 7.4 μm while SO_2 is observed at both 7.4 and 19 μm, i.e. at two slightly different levels, at the cloud top and within the clouds. Following earlier measurements (Fedorova et al. 2008; Krasnopolsky 2010), we assume a D/H value of 200 times the terrestrial value above the clouds.

Figure 13 shows the spectral interval used to retrieve the SO_2 and HDO maps at 7.3 μm, with examples of SO_2 and HDO maps. It was soon realized that both molecules behave very differently (Encrenaz et al. 2012b, 2013). While HDO maps are homogeneous over the disk, SO_2 maps show localized plumes which induce strong variations over the disk, by as much as

a factor 5. Repeated observations over several consecutive hours show that these plumes follow the 4-day rotation of the cloud top, and that their lifetime is limited to a few hours. They were also visible in the 19-μm maps (Encrenaz et al. 2016b). It is interesting to note that the TEXES maps of SO_2 in the infrared range are in very good agreement with the UV maps recorded by the Akatsuki spacecraft (Encrenaz et al. 2019c); this agreement illustrates that the TEXES data can be used to monitor SO_2 on the night side of Venus where UV observations cannot be done.

The existence of the SO_2 plumes was unexpected: since both SO_2 and H_2O are associated with the formation of H_2SO_4, why do we see SO_2 plumes, but no H_2O plumes? According to GCM simulations, the SO_2 plumes are the result of convective motions within the upper cloud (Lefèvre M. et al. 2018, 2020), combined with a strong SO_2 depletion with altitude just above the cloud top; the H_2O mixing ratio, in contrast, is more or less constant in this region, which would explain the absence of H_2O plumes (Lefèvre F., priv. comm.).

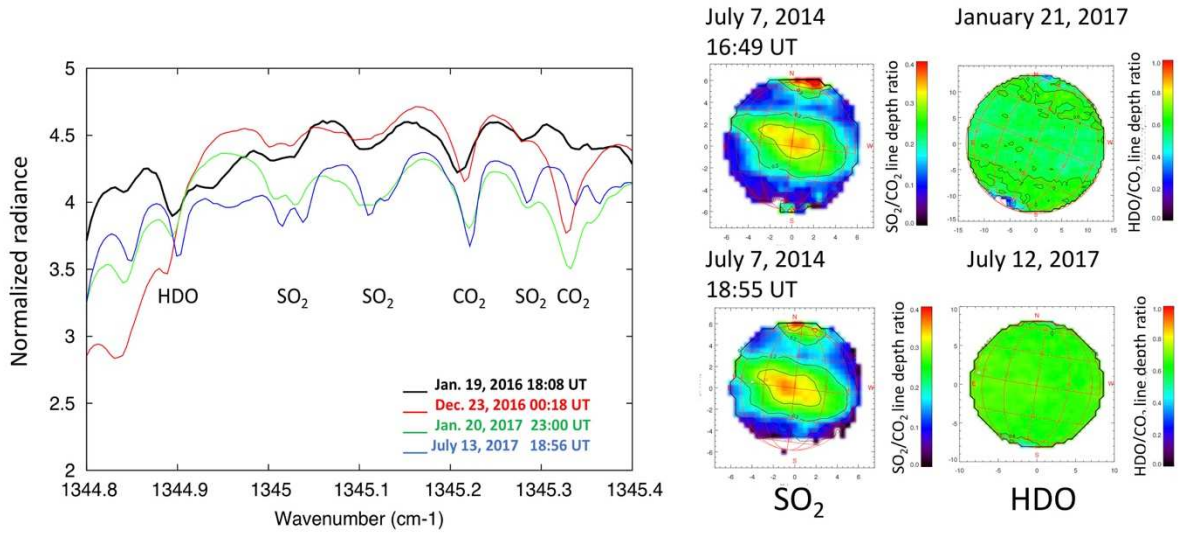

Figure 13. *Left: Examples of disk-integrated TEXES spectra at 7.4 μm, showing weak transitions of SO_2, HDO and CO_2. Right panel: Examples of SO_2 maps (middle column) and HDO maps (right column). The two SO_2 maps are separated by 2 hours. It can be seen that in the second map, the SO_2 plume is shifted by 7.5°, in agreement with the 4-days rotation of the clouds. Source: Encrenaz et al. 2016b, 2019c.*

We have used our whole data base (2012 – 2019) to study the long-term variations of SO_2 and HDO at the cloud top, and we have found a clear anticorrelation (cc = - 0.8; Encrenaz et al. 2020). As shown in Figure 14, this anticorrelation is actually predicted by the dynamical photochemical models of Shao et al. (2021). Between 2014 and 2019, we have observed an overall increase of SO_2 and a slow decrease of H_2O; in 2019, the mixing ratios of both molecules were comparable, at the level of about 500 ppbv, while H_2O was significantly more abundant than SO_2 during the previous years. Unfortunately, no data were obtained in 2020; however, new measurements performed in the summer and fall 2021 indicate that the SO_2 abundance has decreased again. In addition, we have performed a statistical study of the appearance of SO_2 plumes as a function of the local hour. We have shown evidence for a double maximum at the positions of the terminators, which might be the signature of a semi-

diurnal wave (Figure 14). This behavior was also observed, at a slightly higher atmospheric level, by the SPICAV UV experiment (Marcq et al. 2020; Figure 14)

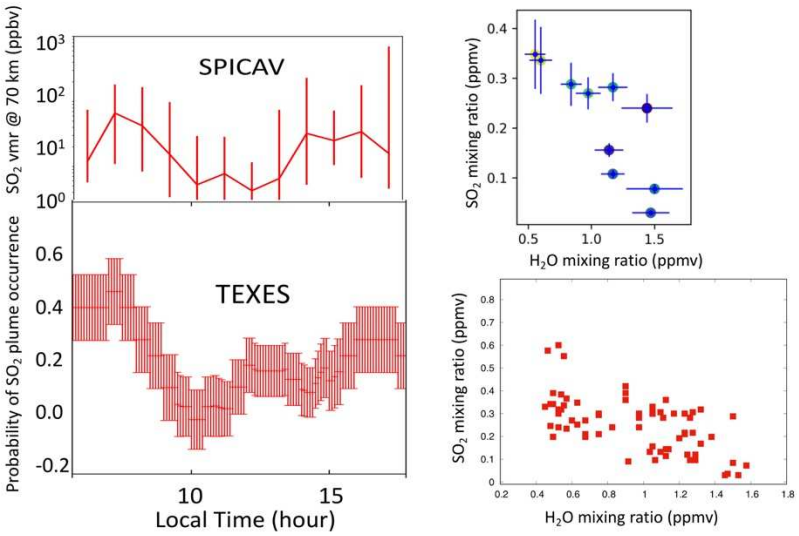

Figure 14. *Left: The distribution of the SO_2 plumes as a function of the local hour, as observed by (top) SPICAV on Venus Express (Marcq et al. 2020), and (bottom) TEXES. Right: The H_2O/SO_2 anticorrelation, as predicted by the models (top, Shao et al. 2021) and as observed by TEXES (bottom; data from Encrenaz et al. 2020b).*

3.2.2 Mesospheric mapping of sulfur and water with ALMA

As mentioned earlier (3.2), the SO_2 vertical distribution is strongly depleted above the clouds, as compared with its tropospheric value. However a second maximum has been detected in the upper mesosphere, at an altitude of about 80 - 90 km by submillimeter measurements of SO and SO_2 (Sandor et al., 2010, 2012). These observations, which exhibit a strong temporal variability, suggest the presence of another sulfur reservoir in the upper mesosphere, possibly in the form of aerosols. In 2011, just before the beginning of our TEXES campaign, we used the ALMA (Atacama Large Millimeter/ submillimeter Array) to map these species; a HDO transition was again used as a proxy to map the water vapor simultaneously. Observations were performed on November 14 and 15, 2011, at frequencies close to 345 GHz (SO and SO_2) and 336 GHz (HDO).

Figure 15 shows the evolution of the SO, SO_2 and HDO maps over 24 hours (Encrenaz et al. 2015). It can be seen that their distributions over the disk are very inhomogeneous, and strongly vary from day to day. The SO transition (also shown in Figure 15) is much stronger than the SO_2 line located in the wing of the SO line, which explains the poor signal-to-noise of the SO_2 map. Still, it can be seen that SO_2 is detected on November 14, but not on November 15. The behavior of water vapor is interesting. It is more or less homogeneous on November 15, but shows a strong localized maximum the day before. There is no apparent correlation between the SO and SO_2 maps, nor between the SO and H_2O maps. As observed at the cloud top, the behavior of SO_2 in the upper atmosphere shows strong local and short-term temporal variations. In contrast, water vapor, which is homogeneous at the cloud top, also shows these local temporal variations in the upper atmosphere. The explanation might be that, at higher

levels, the water vapor content is constrained by its saturation curve; it thus depends upon the mesospheric temperature which is known to exhibit strong daily variations.

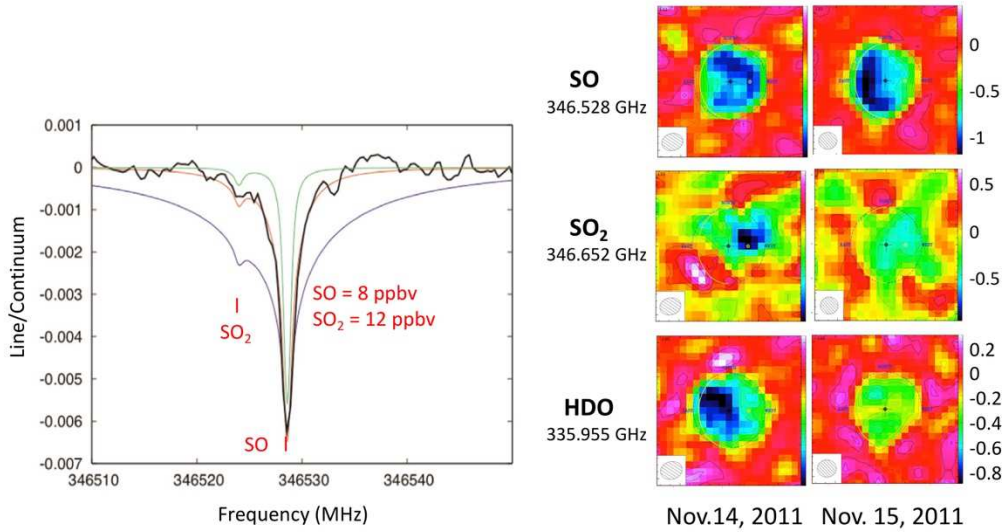

Figure 15. *Left: the SO transition at 346.528 GHz observed on Venus with ALMA on November 14, 2011. A weak transition of SO_2 is visible in the wing of the SO line. The best fit (red curve) is obtained with SO = 8 ppbv and SO_2 = 12 ppbv. Right: maps of SO (top), SO_2 (middle) and HDO (bottom) recorded with ALMA on November 14 and 15, 2011. The unit is the depth of the transition. The blue color indicates a high abundance and the red color corresponds to zero. Source: Encrenaz et al. (2015).*

4. Conclusions and perspectives

This last section reviews some achievements of planetary infrared spectroscopy and some remaining questions, as well as possible future developments, especially in the field of exoplanetary spectroscopy.

4.1 Planetary infrared spectroscopy: a perennial tool

Until the early 1970s, planetary spectroscopy, performed in the visible and near-infrared range, led to the identification of some atmospheric species (CO_2 on Mars and Venus, CH_4 and NH_3 in Jupiter). Absorption lines were observed in front of the reflected solar continuum, leading to an estimate of the abundance of the observed species and (from the line width) the effective pressure of the formation region. After 1973, spectroscopic observations of the Jovian thermal emission became possible in the 4.6-µm and 10-µm windows, leading to the identification of several minor tropospheric and stratospheric species (Figures 1 and 2). Later, thanks to the IRIS instruments of the two Voyager spacecraft, the thermal profile and the H_2/He ratio were retrieved in the atmospheres of the giant planets (Hanel et al. 2003). Later, the use of very high spectral resolution in the millimeter range, using heterodyne spectroscopy, led to the determination of velocity fields on Mars (Moreno et al. 2009). More recently, wind velocities, inferred from high-resolution measurements in the visible range, were measured at the cloud top of Venus (Machado et al. 2017).

Planetary spectroscopy can bring surprises. We have seen the case of the fast response of Jupiter at the time of the SL9 impact (2.2). In several cases, the spectroscopic identification of new species has shown evidence for unexpected physico-chemical processes in planetary atmospheres. It was the case for the detection of phosphine PH_3 on Jupiter (Ridgway et al. 1976), and later Saturn (Tokunaga et al. 1980); this molecule, whose presence is not expected on the basis of thermochemical calculations, has been interpreted as the signature of vertical transport, bringing PH_3 from deep tropospheric levels up to the upper troposphere in a time shorter than the chemical destruction time of the molecule; because of the strong internal source of Saturn (Hanel et al. 1983), probably associated with a stronger vertical transport, this effect is stronger on Saturn than on Jupiter. Another example was the unexpected discovery of a large abundance of CO in the stratosphere on Neptune (Rosenqvist et al. 1992; Marten et al. 1993). In this case, the explanation was the existence of an external oxygen source, later confirmed by the discovery of stratospheric water vapor and carbon dioxide in the stratospheres of the giant planets (Feuchtgruber et al. 1997; 2.3.1). In the case of Neptune, the detection of stratospheric CO and HCN (Marten et al. 1993) and more recently CS Moreno et al. 2017) suggest that a large comet hit the planet within the past thousand years (Lellouch et al. 2005).

4.2 A few open questions…

Regarding the terrestrial planets, there are still open questions about the mechanisms responsible for the diverging evolution of their atmospheres. Some of them are listed below (see, in particular, Esposito et al. 2007, Taylor 2014 and Catling & Kasting 2017).

Did Venus have an early ocean? If yes, could life have appeared and developed before the escape of water? If so, could life have escaped the hostile surface conditions and migrated to the level of the clouds, where temperature and pressure conditions are temperate? Regarding present conditions, is active volcanism responsible for the long-term variations of sulfur dioxide at the cloud top? What are the interaction mechanisms between the surface and the lower atmosphere? What are the sources and sinks of sulfur on Venus, and what is the coupling between the troposphere and the mesosphere? What is the origin of the super-rotation at the cloud top?

Active volcanism at the surface of Venus cannot be traced by the monitoring of sulfur dioxide and water vapor at the cloud top, as performed by SPICAV aboard Venus Express or by TEXES at IRTF. Indeed, as mentioned above (3.2), the short-term SO_2 variability observed by TEXES can be explained by convective motions within the clouds, associated to the steep decrease of SO_2 from below to above the clouds (Lefèvre et al. 2018, 2020); its long-term variability could also possibly be associated with intrinsic variability inside the clouds. Thermal mapping of the surface on the night side, at specific wavelengths located outside the CO_2 absorption bands (0.9, 1.1, 1.7, 2.3 μm) can bring new information on active volcanism through changes of emissivity, as previously reported by Venus Express observations (Smrekar et al. 2010) or variability in the SO_2 and H_2O abundances (Marcq et al. 2021). The best tool for this study, however, will be the Synthetic Aperture Radar (SAR) which is planned aboard the Veritas and EnVision orbiters, to be launched by NASA and ESA respectively for the coming decade.

In the case of Mars, there is a pending problem associated with the paradox of the early faint Sun (see, e.g. Catling & Kasting 2017). When the Sun's radiation was only 70% of its present value, how could the surface temperature be compatible with the presence of liquid water? In contrast with the previous concept of a wet and warm early atmosphere, present models tend to favor a cold and dry environment, with episodic outgassing due to volcanic and/or meteoritic events. Could life have appeared on Mars in such an environment, and if so, could we find extinct or extant traces of it? This quest is triggering the on-going exploration program of Mars.

Also related to this question is the controversy about the possible presence of methane. Since 2003, several ground-based and space observations have reported the sporadic presence of methane (Krasnopolsky et al. 2004, Formisano et al. 2004, Mumma et al. 2009). Because some of these measurements were controversial, and because of their potential implication in terms of astrobiology (the origin of methane on Mars could be either abiotic or biogenic; see e.g. Atreya et al. 2007, 2011), these announcements raised a lot of discussion in the community. A few years later, the Curiosity rover reported again the transient occurrence of methane plumes, over a low persistent background of 0.2 – 0.6 ppbv (Webster et al. 2015, 2021); at the same time, the Trace Gas Orbiter reported a very stringent upper limit, ten times below the background detection of Curiosity (Montmessin et al. 2021). As suggested by Moores et al. (2019), this contradiction could be at least partly due to the day/night cycle of the planetary boundary layer which may be reduced to a few meters during the night (when the CH_4 detection is reported by Curiosity), inhibiting the mixing of methane at higher altitudes (above a few kilometers) where TGO is observing (Webster et al. 2021). The outstanding question regarding methane on Mars is not so much its source (as it could be trapped in clathrates under the surface through abiotic processes) but its fast destruction at the surface. It has been suggested that surface oxidizers, like H_2O_2 or perchlorates ($XClO_4$), could be involved in the destruction of organics at the Martian surface; in particular, large quantities of H_2O_2 could be produced by triboelectric processes at the time of dust storms, and be stored in the regolith (Encrenaz et al. 2012, Atreya et al. 2021). If released at the same time of CH_4 plumes, this oxidizer could rapidly destroy methane at the surface. These coupled surface-atmosphere processes might also explain the discrepancy between the observed H_2O_2 abundance in the gas phase and the model predictions (Section 3.1). It is likely that, in the future, the study of such surface-atmosphere interactions will be crucial for better understanding the seasonal behavior of oxidized species on Mars.

4.3 The future of ground-based planetary spectral mapping

Our observing campaigns on Mars and Venus were performed on a telescope of modest size, the 3-m IRTF, in an excellent high-altitude site, Maunakea Observatory. With the advent of 10-m class telescopes, and the future perspective of ELTs, we could wonder if these spectral mapping programs could benefit from these developments. Actually, the question is already raised since, in a few occasions, the TEXES instrument has been mounted at the 8-m Gemini-N telescope, at the Maunakea observatory.

In the case of large planetary disks (more than ten arcsec in diameter), like Venus, Mars, Jupiter and Saturn, the answer appears to be negative. Indeed, a compromise has to be found between the spectral resolving power (about 80000), the spatial resolution (about 1 arcsec),

the required signal-to-noise (over about 100 per pixel), and the time needed to build a map (typically less than an hour). If a 10-m telescope is used, the number of pixels needed to scan the planet becomes very large and the time needed to build a map becomes prohibitive.

In contrast, the use of TEXES (or similar thermal imaging spectrometers) on 10-m class telescopes is perfectly adapted to the study of small objects, like Io, Titan, or Uranus and Neptune. TEXES has been successfully used at IRTF on Io (Spencer et al. 2005, Tsang et al. 2012, 2013) and on Titan, where two new molecules, propane C_3H_8 and propadiene CH_2CCH_2 were detected (Roe et al. 2003, Lombardo et al. 2019). The use of a larger telescope would allow us to map these species. The spectral mapping of hydrocarbons emissions (CH_4, C_2H_2 and C_2H_6) on Neptune by TEXES at the Gemini telescope has been used to infer the thermal field and the spatial distribution of minor species in the stratosphere of Neptune (Greathouse et al. 2011). Such studies could be developed on large telescopes in the future, and be applied to other objects (Uranus, the icy Galilean satellites, Ceres…).

4.4 From solar system planets to exoplanets

Over the past twenty years, the development of transit spectroscopy of exoplanets has given us some insight into the atmospheric composition of exoplanets. Two methods have been used. In the case of primary transits (when the planet passes in front of its host-star), the atmosphere is observed in transmission at terminator; when it passes behind the star, the dayside emission of the exoplanet is observed. In the second case, the signal is more difficult to observe in the near infrared, but becomes stronger at longer wavelengths as the [planet/star] flux contrast increases (Tinetti et al. 2013). Most of our knowledge on the atmospheric composition of the exoplanets comes from transit observations; however, near-infrared spectroscopy is becoming performed also on young giant exoplanets detected by the imaging technique, and is expected to develop rapidly in the future.

The number of exoplanets where atmospheric species have been detected is close to a hundred. In addition to many atoms (Na, Ca, K, Mg, Fe, O, H, He…), we find several molecules or radicals (H_2O, CH_4, NH_3, CO, CO_2, HCN, C_2H_2, C_2, CN, NH_2…) and more exotic species (AlO, Al_2O_3, SiO, TiO_2, VO…; see Schneider et al. 2011 and http://exoplanet.eu)). It must be noted that these detections can be tentative or questionable; reviews on this topic can be found, in particular, in Seager (2008), Deming and Seager (2017), and Madhusudhan (2019). In addition of the intrinsic weakness of the signal, their identification is made more difficult than in the case of solar system planets for two reasons: (1) hot Jupiters (the easiest targets), as an effect of their high temperature, exhibit broad molecular bands which tend to overlap; (2) in the case of secondary transits, the shapes of the bands (in emission or in absorption) depend upon the thermal profile of the exoplanet which must be simultaneously retrieved.

Can we anticipate the atmospheric composition of a given exoplanet? In the case of a transiting object, we know its mass and its distance to its host-star. Knowing the spectral type of this star, we can estimate the exoplanet's equilibrium temperature. We can then plot a (T, M) diagram and, using solar system objects as analogs, make an initial guess on their atmospheric composition, based on the general laws of thermochemical equilibrium (Tinetti et al. 2013). This diagram, shown in Figure 16, may be used for a very simplified classification of exoplanets.

On the mass scale, the value of 10 terrestrial masses acts as a threshold, because for more massive nuclei, the gravity field is expected to capture the surrounding material (mostly hydrogen and helium) and lead to the formation of a giant planet. Below this threshold, as a first approximation, the planet can be considered as a solid planet. On the temperature scale, a threshold is given by the temperature of the ice line, which can be approximated to the temperature of water condensation in a dilute medium (i.e. about 180 – 200 K). Below this temperature, we expect to have small icy nuclei (Titan, Pluto) or giant planets formed by nuclear accretion. At higher temperature, we expect to have rocky planets (Earth, Mars, Venus or Mercury); the hot exoplanets have no equivalent in the solar system. If we assume the core-accretion scenario for the planetary formation, we do not expect hot giants to be present in this diagram; the existence of hot giant exoplanets is attributed to migration processes.

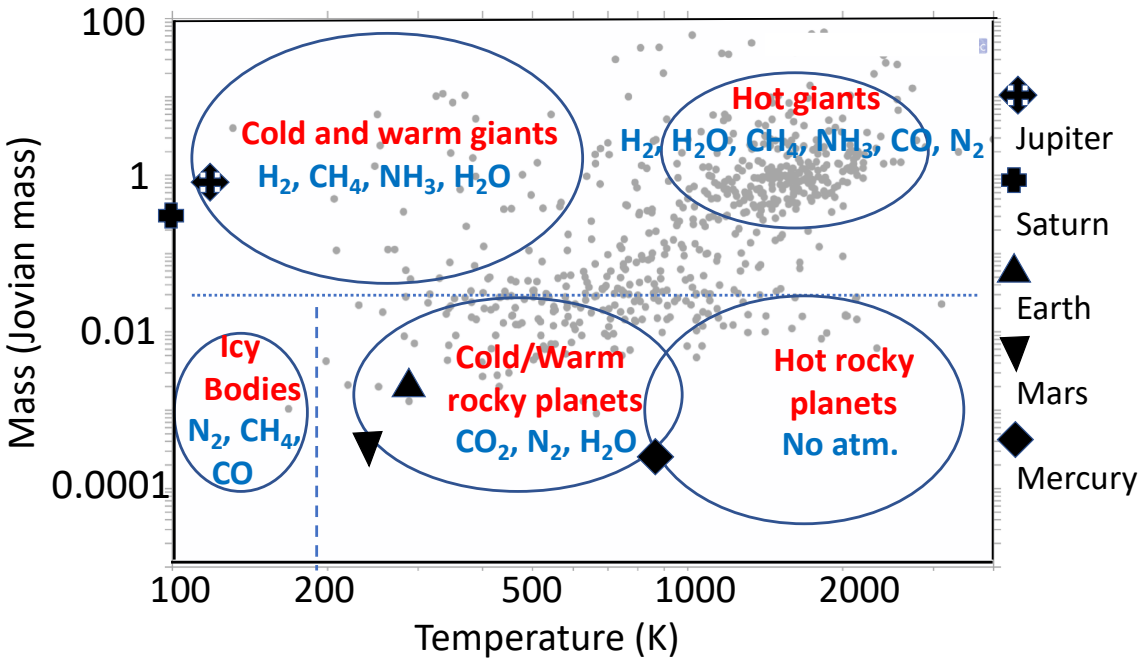

Figure 16. *A classification of exoplanets as a function of temperature and mass. The temperature is the equilibrium temperature, inferred from the distance to the host star and the spectral type of the star. Detected exoplanets are indicated in light grey (Source: exoplanet.eu). The vertical dashed line around T = 200 K indicates the water ice line. The horizontal dotted line indicates the threshold at 10 terrestrial masses, separating solid planets from giant ones. Solar system planets are indicated with black symbols. The hot planets have no equivalent in the solar system. The young giant exoplanets in the process of cooling are missing in this diagram.*

On the basis of this simple diagram, we can estimate what could be the atmospheric composition of each class of exoplanet. Assuming thermochemical equilibrium, we expect carbon (and nitrogen) to be in the form of CH_4 (and NH_3, respectively) at low temperature and high pressure, and in the form of CO or CO_2 (and N_2, respectively) under opposite conditions. This is actually what we observe in the solar system (in the case of the small icy bodies, the presence of nitrogen is explained as the effect of NH_3 photodissociation).

There are several caveats to this very simple classification. The first one is that it does not take into account the effect of migration, which is known to be an efficient mechanism in exoplanetary systems. This is probably the reason why planets of intermediate masses (super-Earths and sub-Neptunes) do not appear on this diagram, while they are known to be very common in the Galaxy (Figure 16). Migration, in particular, could be responsible for the presence of small, very dense exoplanets in the close vicinity of their stars; these objects could be the remnant nuclei of previous massive giant objects, initially formed at large distances (Mocquet et al. 2014). In addition, our diagram does not consider the case of warm young exoplanets, distant from their star, now revealed with imaging techniques. Finally, another caveat is a possible departure from thermochemical equilibrium within the exoplanet's atmospheres: as an example, both CH_4 and CO and have been detected on two giant exoplanets, HD208458b and HD189733b. Nevertheless, in the absence of other constraints, this simple diagram could be considered as a very first step toward the characterization of planetary atmospheres.

Two main mechanisms could be responsible for a departure from thermochemical equilibrium. The first one is photochemistry. In the case of terrestrial planets, it is responsible for the CO_2 and H_2O photodissociation and, in the case of the Earth, for the formation of the ozone layer. In the case of giant planets, it is responsible for the formation of a variety of hydrocarbons from methane photochemistry. The second mechanism is vertical transport, which carries up molecules from the deep troposphere up to observable levels (at pressure levels of a few bars or less) in a lifetime shorter than the destruction lifetime of the molecule. The best example is PH_3 in Jupiter and Saturn (see Section 4.1), and the same situation could occur also on gaseous exoplanets.

In summary, in view of the high diversity of the planetary spectra observed in the solar system – a « simple » multiple system with quasi-coplanar and concentric orbits ! – we must be prepared to discover an extreme variety of exoplanetary spectra. In particular, an important means will be the JWST, starting in 2022. A few years later, the European Ariel mission is expected to provide us with a whole inventory of infrared exoplanetary spectra of all kinds of targets.

5. Acknowledgements

There are many people I am indebted to, and I feel extremely lucky to have met them all. The first one is S. Ichtiaque Rasool who spent a sabbatical year in Paris in 1968, at the time I was a student in astrophysics. He invited me to spend a year at the Goddard Institute for Space Studies and when I came back to Paris Observatory, with Catherine de Bergh and Jean Lecacheux, I became involved in the development of the Planetology Group. In 1972, I spent a year with Toby Owen at the State University of New York at Stony Brook. Toby was a great scientist, both charismatic and visionary, and I always considered him as my advisor.

I am also indebted to the Planetology group of LESIA (Laboratoire d'Etudes et d'Instrumentation en Astrophysique), at Paris Observatory, which has been constantly growing over the past fifty years. Michel Combes played a major role in developing a series of infrared spectrometers which have flown on many spacecraft. Daniel Gautier was one of the

fathers of the Cassini-Huygens mission. I was very lucky to meet excellent students, in particular Pierre Drossart, Emmanuel Lellouch, Bruno Bézard, Athena Coustenis, Thierry Fouchet and Raphaël Moreno who all became close collaborators. Today the “Planeto” group is still growing with many experienced scientists, as well as many young bright students and postdocs. It is a pleasure to work in this environment.

Since the early years of my carrier, I have been observing at Maunakea Observatory. This is a wonderful place and I was always happy to spend a couple of weeks there. Since the early 2000s, I have been using the Texas Echelon Cross Echelle Spectrograph (TEXES) imaging spectrometer at the NASA Infrared Telescope Facility (IRTF), whose director was Alan Tokunaga. I am most grateful to Tommy Greathouse who has been operating TEXES for about twenty years; working with him at IRTF has been (and still is) a great experience.

In 2009, at the occasion of a conference in Barcelona, I started being interested in exoplanets. At this occasion I met Giovanna Tinetti, and I am very grateful to her for having introduced me to the new field of exoplanetary spectroscopy.

I had many friendly and long-lasting collaborations during my career. The first one was with Jean-Pierre Bibring and his group at the Institut d’Astrophysique Spatiale (Orsay, France), as well as Vassili Moroz at the Space Research Institute (IKI) in Moscow. Another one was with the Planetary Group of Jet Propulsion Laboratory, in particular, Glenn Orton and Bob Carlson; I am especially grateful to Sam Gulkis who allowed us (my husband Pierre and me) to come to JPL frequently. I also want to mention my long-term collaboration with Sushil Atreya from the University of Michigan; it is always a pleasure for me to exchange with him and hear his innovative ideas. Over the years, I have also developed a friendly and fruitful collaboration with the team initiated by François Forget in Paris, which includes many bright scientists from LMD (Laboratoire de Météorologie Dynamique) and LATMOS (Laboratoire Atmosphères, Milieux, Observations Spatiales), and has developed Global Climatic Models for most of the planets and satellites with an atmosphere.

Over the three past decades, I have spent quite some time writing text books and popular books. I have been most lucky to meet two very good friends and co-authors whom I want to thank, James Lequeux and Fabienne Casoli, both from Paris Observatory. And, last but not least, my profound thanks to my family, my husband Pierre Encrenaz (a radio-astronomer who turned out to be also a planetologist) and our children and grand-children.

I would like to conclude this paper with a comment. When I started working in astronomy, there were very few women in this field, especially in the US. I remember a conference in the US, in the early 1970s, attended by more than a hundred participants and only three women... I am very happy to see so many young women attending the DPS conference these days, and I hope that this tendency will continue and grow in the future.

I want to thank the DPS Committee for having giving me the 2021 Gerard P. Kuiper prize, and the Icarus Editorial Board for having invited me to write this review. I am very grateful to Julianne Moses and Athena Coustenis for their helpful comments regarding this paper.

6. References

Atreya, S. K., Gu, Z. G. 1994. Stability of the Martian atmosphere: Is heterogeneous catalysis essential?. Journal of Geophysical Research 99, 13133-13146. doi:10.1029/94JE01085

Atreya, S. K. and 7 colleagues 1999. A comparison of the atmospheres of Jupiter and Saturn: deep atmospheric composition, cloud structure, vertical mixing, and origin. Planetary and Space Science 47, 1243-1262. doi:10.1016/S0032-0633(99)00047-1

Atreya, S. K., Mahaffy, P. R., Wong, A.-S. 2007. Methane and related trace species on Mars: Origin, loss, implications for life, and habitability. Planetary and Space Science 55, 358-369. doi:10.1016/j.pss.2006.02.005

Atreya, S. K. and 7 colleagues 2011. Methane on Mars: Current observations, interpretation, and future plans. Planetary and Space Science 59, 133-136. doi:10.1016/j.pss.2010.10.008

Atreya, S. K., Webster, C., Mahaffy, P., Wong, M., Trainer, M. 2021. Unexpected Seasonal Increase in Oxygen on Mars: Possible Role of Coupled Surface-Atmosphere Processes**.** 43rd COSPAR Scientific Assembly. Held 28 January - 4 February, 2021. Abstract F3.3-0001-21 (oral), id.1937.

Baines, K. H., Hammel, H. B., Rages, K. A., Romani, P. N., Samuelson, R. E. 1995. Clouds and hazes in the atmosphere of Neptune. Neptune and Triton, 489-546.

Baines, K. H., Mickelson, M. E., Larson, L. E., Ferguson, D. W. 1995. The Abundances of Methane and Ortho/Para Hydrogen on Uranus and Neptune: Implications of New Laboratory 4-0 H_2 Quadrupole Line Parameters. Icarus 114, 328-340. doi:10.1006/icar.1995.1065

Belyaev, D. A. and 8 colleagues 2012. Vertical profiling of SO_2 and SO above Venus' clouds by SPICAV/SOIR solar occultations. Icarus 217, 740-751. doi:10.1016/j.icarus.2011.09.025

Bézard, B., de Bergh, C., Crisp, D., Maillard, J.-P. 1990. The deep atmosphere of Venus revealed by high-resolution nightside spectra. Nature 345, 508511. doi:10.1038/345508a0

Bézard, B. 2000. Spectroscopy of Solar System Objects. ISO Beyond the Peaks: The 2nd ISO Workshop on Analytical Spectroscopy, ESA-SP456, p. 3

Bézard, B., Feuchtgruber, H., Moses, J. I., Encrenaz, T. 1998. Detection of methyl radicals (CH_3) on Saturn. Astronomy and Astrophysics 334, L41-L44.

Bézard, B., Romani, P. N., Feuchtgruber, H., Encrenaz, T. 1999. Detection of the Methyl Radical on Neptune. The Astrophysical Journal 515, 868-872. doi:10.1086/307070

Bézard, B., Droosart, P., Encrenaz, T., Feuchtgruber, H. 2001. Benzene on the giant planets. Icarus. 154, 492-500. doi: 10.1006/icar.2001.6719

Bézard, B., de Bergh, C. 2007. Composition of the atmosphere of Venus below the clouds. Journal of Geophysical Research (Planets) 112. doi:10.1029/2006JE002794

1186 Cameron, A. G. W. 1973. Accumulation processes in the primitive solar nebula. Icarus 18,
1187 407-450. doi:10.1016/0019-1035(73)90153- X

1188 Cameron, A. G. W., Pine, M. R. 1973. Numerical models of the primitive solar nebula. Icarus
1189 18, 377-406. doi:10.1016/0019- 1035(73)90152-8

1190 Cameron, A. G. W. 1988. Origin of the solar system.. Annual Review of Astronomy and
1191 Astrophysics 26, 441-472. doi:10.1146/annurev.aa.26.090188.002301

1192 Carlson, R. W. and 9 colleagues 1995. Galileo infrared observations of the Shoemaker-Levy G
1193 impact fireball: A preliminary report. Geophysical Research Letters 22, 1157-1160.

1194 Catling, D. C., Kasting, J. F. 2017. Atmospheric Evolution on Inhabited and Lifeless Worlds, by
1195 David C. Catling, James F. Kasting, Cambridge, UK: Cambridge University Press, 2017.

1196 Cavalié, T. and 13 colleagues 2013. Spatial distribution of water in the stratosphere of Jupiter
1197 from Herschel HIFI and PACS observations. Astronomy and Astrophysics 553.
1198 doi:10.1051/0004-6361/201220797

1199 Cavalié,T.and 10 colleagues 2014. The first submillimeter observation of CO in the
1200 stratosphere of Uranus. Astronomy and Astrophysics 562. doi:10.1051/0004-
1201 6361/201322297

1202 Clancy, R. T., Sandor, B. J., Moriarty-Schieven, G. H. 2004. A measurement of the 362 GHz
1203 absorption line of Mars atmospheric H_2O_2. Icarus 168, 116-121.
1204 doi:10.1016/j.icarus.2003.12.003

1205 Combes, M., Encrenaz, T., Owen, T. 1978. On the abundance of deuterium in Jupiter's
1206 atmosphere.. The Astrophysical Journal 221, 378-381. doi:10.1086/156036

1207 Combes, M., Encrenaz, T. 1979. A method for the determination of abundance ratios in the
1208 outer planets—Application to Jupiter. Icarus 39, 1-27. doi:10.1016/0019-1035(79)90096-4

1209 Connes, J., Connes, P., Maillard, J.-P. 1969. Atlas des spectres dans le proche infrarouge de
1210 Vénus, Mars, Jupiter et Saturne., by Connes, J., Connes, P., Maillard, J.-P.. Paris (France):
1211 Editions du Centre National de la Recherche Scientifique, 471 p..

1212 Coustenis, A. and 8 colleagues 1998. Evidence for water vapor in Titan's atmosphere from
1213 ISO/SWS data. Astronomy and Astrophysics 336, L85-L89.

1214 Daerden, F. and 7 colleagues 2019. Mars atmospheric chemistry simulations with the GEM-
1215 Mars general circulation model. Icarus 326, 197-224. doi:10.1016/j.icarus.2019.02.030

1216 de Graauw, T. and 61 colleagues 1996. Observing with the ISO Short-Wavelength
1217 Spectrometer.. Astronomy and Astrophysics 315, L49-L54.

1218 de Graauw, T. and 18 colleagues 1997. First results of ISO-SWS observations of Saturn:
1219 detection of CO_2, CH_3C_2H, C_4H_2 and tropospheric H_2O. Astronomy and Astrophysics 321, L13-
1220 L16.

1221 Deming, L. D., Seager, S. 2017. Illusion and reality in the atmospheres of exoplanets. Journal
1222 of Geophysical Research (Planets) 122, 53-75. doi:10.1002/2016JE005155

1223 de Pater, I. and 8 colleagues 2014. Neptune's global circulation deduced from multi-
1224 wavelength observations. Icarus 237, 211-238. doi:10.1016/j.icarus.2014.02.030

1225 Drossart, P. and 11 colleagues 1989. Detection of H_3^+ on Jupiter. Nature 340, 539-541.
1226 doi:10.1038/340539a0

1227 Drossart, P. and 6 colleagues 1999. Fluorescence in the 3μm bands of methane on Jupiter
1228 and Saturn from ISO/SWS observations. The Universe as Seen by ISO, ESA-SP427, p. 169.

1229 Encrenaz, T. 2008. Water in the solar system. Annual Review of Astronomy and Astrophysics
1230 46, 57-87. doi:10.1146/annurev.astro.46.060407.145229

1231 Encrenaz, T., Combes, M., Zéau, Y. 1978. The Spectrum of Jupiter between 10 and 13 μm .
1232 Astronomy and Astrophysics 70, 29-36.

1233 Encrenaz, T., Combes, M., Zéau, Y. 1980. The spectrum of Jupiter between 8 and 9 microns -
1234 Estimates of the Jovian C/H and D/H ratios. Astronomy and Astrophysics 84, 148-153.

1235 Encrenaz, T., Schulz, R., Stüwe, J. A., Wiedemann, G., Drossart, P., Crovisier, J. 1995. Near-ir
1236 spectroscopy of Jupiter at the time of comet Shoemaker-Levy 9 Impacts: Emissions of CH_4,
1237 H_3^+ and H_2. Geophysical Research Letters 22, 1577-1580. doi:10.1029/95GL00810

1238 Encrenaz, T. and 19 colleagues 1996. First results of ISO-SWS observations of Jupiter.
1239 Astronomy and Astrophysics 315, L397-L400.

1240 Encrenaz, T., Drossart, P., Carlson, R. W., Bjoraker, G. 1997. Detection of H_2O in the splash
1241 phase of G- and R-impacts from NIMS-Galileo. Planetary and Space Science 45, 1189-1196.
1242 doi:10.1016/S0032-0633(97)00025-1

1243 Encrenaz, T. and 6 colleagues 2002. A stringent upper limit of the H_2O_2 abundance in the
1244 Martian atmosphere. Astronomy and Astrophysics 396, 1037-1044. doi:10.1051/0004-
1245 6361:20021465

1246 Encrenaz, T. 2003. ISO observations of the giant planets and Titan: what have we learnt?.
1247 Planetary and Space Science 51, 89-103. doi:10.1016/S0032-0633(02)00145-9

1248 Encrenaz, T., Drossart, P., Orton, G., Feuchtgruber, H., Lellouch, E., Atreya, S. K. 2003. The
1249 rotational temperature and column den- sity of H_3^+ in Uranus. Planetary and Space Science
1250 51, 1013-1016. doi:10.1016/j.pss.2003.05.010

1251 Encrenaz, T., Lellouch, E., Drossart, P., Feuchtgruber, H., Orton, G. S., Atreya, S. K. 2004. First
1252 detection of CO in Uranus. Astronomy and Astrophysics 413, L5-L9. doi:10.1051/0004-
1253 6361:20034637

1254 Encrenaz, T. and 9 colleagues 2004. Hydrogen peroxide on Mars: evidence for spatial and
1255 seasonal variations. Icarus 170, 424-429. doi:10.1016/j.icarus.2004.05.008

1256 Encrenaz, T. and 10 colleagues 2005. Infrared imaging spectroscopy of Mars: H_2O mapping
1257 and determination of CO_2 isotopic ratios. Icarus 179, 43-54. doi:10.1016/j.icarus.2005.06.022

1258 Encrenaz, T. and 9 colleagues 2008. Simultaneous mapping of H_2O and H_2O_2 on Mars from
1259 infrared high-resolution imaging spectroscopy. Icarus 195, 547-556.
1260 doi:10.1016/j.icarus.2008.01.022

1261 Encrenaz, T. and 11 colleagues 2010. Water vapor map of Mars near summer solstice using
1262 ground-based infrared spectroscopy. Astronomy and Astrophysics 520. doi:10.1051/0004-
1263 6361/200913905

1264 Encrenaz, T. and 8 colleagues 2011. A stringent upper limit to SO_2 in the Martian
1265 atmosphere. Astronomy and Astrophysics 530. doi:10.1051/0004-6361/201116820

1266 Encrenaz, T., Greathouse, T. K., Lefèvre, F., Atreya, S. K. 2012. Hydrogen peroxide on Mars:
1267 Observations, interpretation and future plans. Planetary and Space Science 68, 3-17.
1268 doi:10.1016/j.pss.2011.03.019

1269 Encrenaz, T. and 7 colleagues 2012. HDO and SO_2 thermal mapping on Venus: evidence for
1270 strong SO_2 variability. Astronomy and Astrophysics 543. doi:10.1051/0004-6361/201219419

1271 Encrenaz, T. and 8 colleagues 2013. HDO and SO_2 thermal mapping on Venus. II. The SO_2
1272 spatial distribution above and within the clouds. Astronomy and Astrophysics 559.
1273 doi:10.1051/0004-6361/201322264

1274 Encrenaz, T., Moreno, R., Moullet, A., Lellouch, E., Fouchet, T. 2015. Submillimeter mapping
1275 of mesospheric minor species on Venus with ALMA. Planetary and Space Science 113, 275-
1276 291. doi:10.1016/j.pss.2015.01.011

1277 Encrenaz, T. and 8 colleagues 2016. HDO and SO_2 thermal mapping on Venus. III. Short-term
1278 and long-term variations between 2012 and 2016. Astronomy and Astrophysics 595.
1279 doi:10.1051/0004-6361/201628999

1280 Encrenaz, T. and 10 colleagues 2018. New measurements of D/H on Mars using EXES aboard
1281 SOFIA. Astronomy and Astrophysics 612. doi:10.1051/0004-6361/201732367

1282 Encrenaz, T. and 14 colleagues 2019. Ground-based infrared mapping of H_2O_2 on Mars near
1283 opposition. Astronomy and Astrophysics 627. doi:10.1051/0004-6361/201935300

Encrenaz, T. and 10 colleagues 2018. New measurements of D/H on Mars using EXES aboard SOFIA. Astronomy and Astrophysics 612. doi:10.1051/0004-6361/201732367

Encrenaz, T. and 15 colleagues 2020. HDO and SO_2 thermal mapping on Venus. V. Evidence for a long-term anti-correlation. Astronomy and Astrophysics 639. doi:10.1051/0004-6361/202037741

Encrenaz, T. and 9 colleagues 2020. A stringent upper limit of the PH_3 abundance at the cloud top of Venus. Astronomy and Astrophysics 643. doi:10.1051/0004-6361/202039559

Esposito, L. W. 1984. Sulfur Dioxide: Episodic Injection Shows Evidence for Active Venus Volcanism. Science 223, 1072-1074. doi:10.1126/science.223.4640.1072

Fedorova, A. and 10 colleagues 2008. HDO and H_2O vertical distributions and isotopic ratio in the Venus mesosphere by Solar Occultation at Infrared spectrometer on board Venus Express. Journal of Geophysical Research (Planets) 113. doi:10.1029/2008JE003146

Feuchtgruber, H., Lellouch, E., de Graauw, T., Be´zard, B., Encrenaz, T., Griffin, M. 1997. External supply of oxygen to the atmospheres of the giant planets. Nature 389, 159-162. doi:10.1038/38236

Feuchtgruber,H.,Lellouch,E., Bézard,B., Encrenaz, T., de Graauw, T., Davis, G. R. 1999. Detection of HD in the atmospheres of Uranus and Neptune: a new determination of the D/H ratio. Astronomy and Astrophysics 341, L17-L21.

Feuchtgruber, H. and 8 colleagues 1999. Oxygen in the stratospheres of the giant planets and Titan. The Universe as Seen by ISO, ESA-SP427, p. 133.

Feuchtgruber, H. and 11 colleagues 2013. The D/H ratio in the atmospheres of Uranus and Neptune from Herschel-PACS observations. Astronomy and Astrophysics 551. doi:10.1051/0004- 6361/201220857

Forget, F. and 8 colleagues 1999. Improved general circulation models of the Martian atmosphere from the surface to above 80 km. Journal of Geophysical Research 104, 24155-24176. doi:10.1029/1999JE001025

Formisano, V., Atreya, S., Encrenaz, T., Ignatiev, N., Giuranna, M. 2004. Detection of Methane in the Atmosphere of Mars. Science 306, 1758-1761. doi:10.1126/science.1101732

Fouchet, T., Lellouch, E. 2000. Vapor Pressure Isotope Fractionation Effects in Planetary Atmospheres: Application to Deuterium. Icarus 144, 114-123. doi:10.1006/icar.1999.6264

Gillett, F. C., Low, F. J., Stein, W. A. 1969. The 2.8-14-micron Spectrum of Jupiter. The Astrophysical Journal 157, 925. doi:10.1086/150124

Gilli, G. and 7 colleagues 2021. Venus upper atmosphere revealed by a GCM: II. Model validation with temperature and density measurements. Icarus 366. doi:10.1016/j.icarus.2021.114432

1319 Greathouse, T. K. and 7 colleagues 2011. A spatially resolved high spectral resolution study
1320 of Neptune's stratosphere. Icarus 214, 606-621. doi:10.1016/j.icarus.2011.05.028

1321 Guillot, T. 2019. Signs that Jupiter was mixed by a giant impact. Nature 572, 315-317.
1322 doi:10.1038/d41586-019-02401-1

1323 Hallis, L. J. and 6 colleagues 2012. Hydrogen isotope analyses of alteration phases in the
1324 nakhlite martian meteorites. Geochimica et Cosmochimica Acta 97, 105-119.
1325 doi:10.1016/j.gca.2012.08.017

1326 Hanel, R. A., Conrath, B. J., Kunde, V. G., Pearl, J. C., Pirraglia, J. A. 1983. Albedo, internal
1327 heat flux, and energy balance of Saturn. Icarus 53, 262-285. doi:10.1016/0019-
1328 1035(83)90147-1

1329 Hanel, R. A., Conrath, B. J., Jennings, D. E., Samuelson, R. E. 2003. Exploration of the Solar
1330 System by Infrared Remote Sensing: Second Edition.pp. 534. ISBN 0521818974. Cambridge,
1331 UK: Cambridge University Press, April 2003. 534.

1332 Hartogh, P. and 49 colleagues 2010. Herschel/HIFI observations of Mars: First detection of
1333 O_2 at submillimetre wavelengths and upper limits on HCl and H_2O_2 . Astronomy and
1334 Astrophysics 521. doi:10.1051/0004-6361/201015160

1335 Jakosky, B. M., Farmer, C. B. 1982. The seasonal and global behavior of water vapor in the
1336 Mars atmosphere - Complete global results of the Viking atmospheric water detector
1337 experiment. Journal of Geophysical Research 87, 29993019. doi:10.1029/JB087iB04p02999

1338 Karkoschka, E., Tomasko, M. G. 2011. The haze and methane distributions on Neptune from
1339 HST-STIS spectroscopy. Icarus 211, 780-797. doi:10.1016/j.icarus.2010.08.013

1340 Krasnopolsky, V. A. 1995. Uniqueness of a solution of a steady state photo- chemical
1341 problem: Applications to Mars. Journal of Geophysical Research 100, 3263-3276.
1342 doi:10.1029/94JE03283

1343 Krasnopolsky, V. A. 2002. Mars' upper atmosphere and ionosphere at low, medium, and high
1344 solar activities: Implications for evolution of water. Journal of Geophysical Research (Planets)
1345 107. doi:10.1029/2001JE001809

1346 Krasnopolsky, V. A. 2010. Spatially-resolved high-resolution spectroscopy of Venus 2.
1347 Variations of HDO, OCS, and SO_2 at the cloud tops. Icarus 209, 314-322.
1348 doi:10.1016/j.icarus.2010.05.008

1349 Krasnopolsky, V. A. 2015. Variations of the HDO/H_2O ratio in the martian atmosphere and
1350 loss of water from Mars. Icarus 257, 377-386. doi:10.1016/j.icarus.2015.05.021

1351 Krasnopolsky, V. A., Bjoraker, G. L., Mumma, M. J., Jennings, D. E. 1997. High-resolution
1352 spectroscopy of Mars at 3.7 and 8 μm: A sensitive search of H_2O_2 , H_2CO, HCl, and CH_4 , and
1353 detection of HDO. Journal of Geophysical Research 102, 6525-6534. doi:10.1029/96JE03766

1354 Krasnopolsky, V. A., Maillard, J. P., Owen, T. C. 2004. Detection of methane in the Martian
1355 atmosphere: evidence for life?. Icarus 172, 537-547. doi:10.1016/j.icarus.2004.07.004

1356 Lacy, J. H., Richter, M. J., Greathouse, T. K., Jaffe, D. T., Zhu, Q. 2002. TEXES: A Sensitive High-
1357 Resolution Grating Spectrograph for the Mid-Infrared. Publications of the Astronomical
1358 Society of the Pacific 114, 153-168. doi:10.1086/338730

1359 Lagage, P. O. and 25 colleagues 2004. Successful Commissioning of VISIR: The Mid-Infrared
1360 VLT Instrument. The Messenger 117, 1216.

1361 Lebonnois, S., Sugimoto, N., Gilli, G. 2016. Wave analysis in the atmosphere of Venus below
1362 100-km altitude, simulated by the LMD Venus GCM. Icarus 278, 38-51.
1363 doi:10.1016/j.icarus.2016.06.004

1364 Lefèvre, F. and 8 colleagues 2008. Heterogeneous chemistry in the atmosphere of Mars.
1365 Nature 454, 971-975. doi:10.1038/nature07116

1366 Lefèvre, M., Lebonnois, S., Spiga, A. 2018. Three-Dimensional Turbulence- Resolving
1367 Modeling of the Venusian Cloud Layer and Induced Gravity Waves: Inclusion of Complete
1368 Radiative Transfer and Wind Shear. Journal of Geophysical Research (Planets) 123, 2773-
1369 2789.doi:10.1029/2018JE005679

1370 Lefèvre,M., Spiga,A., Lebonnois, S. 2020. Mesoscale modeling of Venus' bow-shape waves.
1371 Icarus 335. doi:10.1016/j.icarus.2019.07.010

1372 Lellouch, E. and 13 colleagues 1995. Chemical and thermal response of Jupiter's atmosphere
1373 following the impact of comet Shoemaker- Levy 9. Nature 373, 592-595.
1374 doi:10.1038/373592a0

1375 Lellouch, E., Bézard,B., Fouchet,T., Feuchtgruber,H., Encrenaz,T., de Graauw, T. 2001. The
1376 deuterium abundance in Jupiter and Saturn from ISO-SWS observations. Astronomy and
1377 Astrophysics 370, 610-622. doi:10.1051/0004-6361:20010259

1378 Lellouch, E. and 8 colleagues 2002. The Origin of Water Vapor and Carbon Dioxide in
1379 Jupiter's Stratosphere. Icarus 159, 112-131. doi:10.1006/icar.2002.6929

1380 Lellouch, E. and 8 colleagues 2015. New constraints on the CH_4 vertical profile in Uranus and
1381 Neptune from Herschel observations. Astronomy and Astrophysics 579. doi:10.1051/0004-
1382 6361/201526518

1383 Lombardo, N. A. and 10 colleagues 2019. Detection of Propadiene on Titan. The
1384 Astrophysical Journal 881. doi:10.3847/2041-8213/ab3860

1385 Machado, P., Widemann, T., Peralta, J., Gonc¸alves, R., Donati, J.-F., Luz, D. 2017. Venus
1386 cloud-tracked and doppler velocimetry winds from CFHT/ESPaDOnS and Venus
1387 Express/VIRTIS in April 2014. Icarus 285, 8-26. doi:10.1016/j.icarus.2016.12.017

1388 Madhusudhan, N. 2019. Exoplanetary Atmospheres: Key Insights, Challenges, and Prospects.
1389 Annual Review of Astronomy and Astrophysics 57, 617-663. doi:10.1146/annurev-astro-
1390 081817- 051846

1391 Mahaffy, P. R. and 27 colleagues 2015. The imprint of atmospheric evolution in the D/H of
1392 Hesperian clay minerals on Mars. Science 347, 412-414. doi:10.1126/science.1260291

1393 Marcq, E. and 6 colleagues 2011. An investigation of the SO_2 content of the venusian
1394 mesosphere using SPICAV-UV in nadir mode. Icarus 211, 58-69.
1395 doi:10.1016/j.icarus.2010.08.021

1396 Marcq, E., Bertaux, J.-L., Montmessin, F., Belyaev, D. 2013. Variations of sulphur dioxide at
1397 the cloud top of Venus's dynamic atmosphere. Nature Geoscience 6, 25-28.
1398 doi:10.1038/ngeo1650

1399 Marcq, E. and 8 colleagues 2020. Climatology of SO_2 and UV absorber at Venus' cloud top
1400 from SPICAV-UV nadir dataset. Icarus 335. doi:10.1016/j.icarus.2019.07.002

1401 Marten, A. and 7 colleagues 1993. First Observations of CO and HCN on Neptune and Uranus
1402 at Millimeter Wavelengths and Their Implications for Atmospheric Chemistry. The
1403 Astrophysical Journal 406, 285. doi:10.1086/172440

1404 Merlivat, L., Nief, G. 1967. Fractionnement isotopique lors des changements d'état solide-
1405 vapeur et liquide- vapeur de l'eau à des températures inférieures à 0°C. Tellus 19, 122127.
1406 doi:10.3402/tellusa.v19i1.9756

1407 Mizuno, H. 1980. Formation of the Giant Planets. Progress of Theoretical Physics 64, 544-
1408 557. doi:10.1143/PTP.64.544

1409 Mocquet, A., Grasset, O., Sotin, C. 2014. Very high-density planets: a possible remnant of gas
1410 giants. Philosophical Transactions of the Royal Society of London Series A 372, 20130164-
1411 20130164. doi:10.1098/rsta.2013.0164

1412 Montmessin, F., Fouchet, T., Forget, F. 2005. Modeling the annual cycle of HDO in the
1413 Martian atmosphere. Journal of Geophysical Research (Planets) 110.
1414 doi:10.1029/2004JE002357

1415 Montmessin, F. and 19 colleagues 2021. A stringent upper limit of 20 pptv for methane on
1416 Mars and constraints on its dispersion outside Gale crater. Astronomy and Astrophysics 650.
1417 doi:10.1051/0004- 6361/202140389

1418 Moores, J. E. and 10 colleagues 2019. The Methane Diurnal Variation and Microseepage Flux
1419 at Gale Crater, Mars as Constrained by the ExoMars Trace Gas Orbiter and Curiosity
1420 Observations. Geophysical Research Letters 46, 9430-9438. doi:10.1029/2019GL083800

1421 Moreno, R., Lellouch, E., Forget, F., Encrenaz, T., Guilloteau, S., Millour, E. 2009. Wind
1422 measurements in Mars' middle atmosphere: IRAM Plateau de Bure interferometric CO
1423 observations. Icarus 201, 549-563. doi:10.1016/j.icarus.2009.01.027

1424 Moreno, R., Lellouch, E., Cavalié, T., Moullet, A. 2017. Detection of CS in Neptune's
1425 atmosphere from ALMA observations. Astronomy and Astrophysics 608. doi:10.1051/0004-
1426 6361/201731472

1427 Moses, J. I., Be ́zard, B., Lellouch, E., Gladstone, G. R., Feuchtgruber, H., Allen, M. 2000.
1428 Photochemistry of Saturn's Atmosphere. I. Hydrocarbon Chemistry and Comparisons with
1429 ISO Observations. Icarus 143, 244-298. doi:10.1006/icar.1999.6270

1430 Moses, J. I., Lellouch, E., Be ́zard, B., Gladstone, G. R., Feuchtgruber, H., Allen, M. 2000.
1431 Photochemistry of Saturn's Atmosphere. II. Effects of an Influx of External Oxygen. Icarus
1432 145, 166-202. doi:10.1006/icar.1999.6320

1433 Mumma, M. J. and 7 colleagues 2009. Strong Release of Methane on Mars in Northern
1434 Summer 2003. Science 323, 1041. doi:10.1126/science.1165243

1435 Nair, H., Allen, M., Anbar, A. D., Yung, Y. L., Clancy, R. T. 1994. A Photochemical Model of the
1436 Martian Atmosphere. Icarus 111, 124-150. doi:10.1006/icar.1994.1137

1437 Navarro, T., Gilli, G., Schubert, G., Lebonnois, S., Lefèvre, F., Quirino, D. 2021. Venus' upper
1438 atmosphere revealed by a GCM: I. Structure and variability of the circulation. Icarus 366.
1439 doi:10.1016/j.icarus.2021.114400

1440 Noll, K. S., Weaver, H. A., Feldman, P. D. 1996. The Collision of Comet Shoemaker-Levy 9 and
1441 Jupiter. IAU Colloq. 156: The Collision of Comet Shoemaker-Levy 9 and Jupiter, 387.

1442 Orton, G. S., Encrenaz, T., Leyrat, C., Puetter, R., Friedson, A. J. 2007. Evidence for methane
1443 escape and strong seasonal and dynamical perturbations of Neptune's atmospheric
1444 temperatures. Astronomy and Astrophysics 473, L5-L8. doi:10.1051/0004-6361:20078277

1445 Orton, G. S. and 6 colleagues 2015. Thermal imaging of Uranus: Upper-tropospheric
1446 temperatures one season after Voyager. Icarus 260, 94-102.
1447 doi:10.1016/j.icarus.2015.07.004

1448 Owen, T., Maillard, J. P., de Bergh, C., Lutz, B. L. 1988. Deuterium on Mars: The Abundance
1449 of HDO and the Value of D/H. Science 240, 1767-1770. doi:10.1126/science.240.4860.1767

1450 Owen, T. and 6 colleagues 1999. A low-temperature origin for the planetesimals that formed
1451 Jupiter. Nature 402, 269-270. doi:10.1038/46232

1452 Owen, T., Encrenaz, T. 2006. Compositional constraints on giant planet formation. Planetary
1453 and Space Science 54, 1188-1196. doi:10.1016/j.pss.2006.05.030

1454 Oyama, V. I., Berdahl, B. J. 1977. The Viking gas exchange experiment results from Chryse
1455 and Utopia surface samples. Journal of Geophysical Research 82, 4669-4676.
1456 doi:10.1029/JS082i028p04669

Pollack, J. B., Hubickyj, H., Bodenheimer, P.,Lissauer, J. J., Podolak, M., Greenzweig, Y. 1996. Formation of giant planets by concurrent accretion of solids and gas. Icarus 124, 62-85. doi: 10.1006/icar.1996.0190

Prinn, R. G., Fegley, B. 1987. The Atmospheres of Venus, Earth, and Mars: a Critical Comparison. Annual Review of Earth and Planetary Sciences 15, 171. doi:10.1146/annurev.ea.15.050187.001131

Rayner, J. and 7 colleagues. 2003. SpeX: A Medium-Resolution 0.8-5.5 Micron Spectrograph and Imager for the NASA Infrared Telescope Facility**.** Publications of the Astronomical Society of the Pacific 115, 362-382. doi:10.1086/367745

•

Ridgway, S. T., Wallace, L., Smith, G. R. 1976. The 800 - 1200 inverse centimeter absorption spectrum of Jupiter.. The Astrophysical Journal 207, 1002-1006. doi:10.1086/154570

Roe, H. G., Greathouse, T. K., Richter, M. J., Lacy, J. H. 2003. Propane on Titan. The Astrophysical Journal 597, L65-L68. doi:10.1086/379816

Rosenqvist, J., Lellouch, E., Romani, P. N., Paubert, G., Encrenaz, T. 1992. Millimeter-Wave Observations of Saturn, Uranus, and Neptune: CO and HCN on Neptune. The Astrophysical Journal 392, L99. doi:10.1086/186435

Sandor, B. J., Todd Clancy, R., Moriarty-Schieven, G., Mills, F. P. 2010. Sulfur chemistry in the Venus mesosphere from SO_2 and SO microwave spectra. Icarus 208, 49-60. doi:10.1016/j.icarus.2010.02.013

Sandor, B. J., Clancy, R. T., Moriarty-Schieven, G. 2012. Upper limits for H_2SO_4 in the mesosphere of Venus. Icarus 217, 839-844. doi:10.1016/j.icarus.2011.03.032

Schneider, J., Dedieu, C., Le Sidaner, P., Savalle, R., Zolotukhin, I. 2011. Defining and cataloging exoplanets: the exoplanet.eu database. Astronomy and Astrophysics 532. doi:10.1051/0004-6361/201116713

Schulz, R., Encrenaz, T., Stüwe, J. A., Wiedemann, G. 1995. Near-IR emissions in the upper Jovian atmosphere after SL-9 impact: Indications of possible northern counterparts. Geophysical Research Letters 22, 2421-2424. doi:10.1029/95GL02286

Schulz, B., Encrenaz, T., Bézard, B., Romani, P. N., Lellouch, E., Atreya, S. K. 1999. Detection of C_2H_4 in Neptune from ISO/PHT-S observations. Astronomy and Astrophysics 350, L13-L17.

Seager, S. 2008. Exoplanet Transit Spectroscopy and Photometry. Space Science Reviews 135, 345-354. doi:10.1007/s11214-008- 9308-5

Shao, W. D., Zhang, X., Bierson, C. J., Encrenaz, T. 2020. Revisiting the Sulfur-Water Chemical System in the Middle Atmosphere of Venus. Journal of Geophysical Research (Planets) 125. doi:10.1029/2019JE006195

Smith, M. D. 2002. The annual cycle of water vapor on Mars as observed by the Thermal Emission Spectrometer. Journal of Geophysical Research (Planets) 107. doi:10.1029/2001JE001522

Smith, M. D. 2004. Interannual variability in TES atmospheric observations of Mars during 1999-2003. Icarus 167, 148-165. doi:10.1016/j.icarus.2003.09.010

Smrekar, S. E. and 7 col- leagues 2010. Recent Hotspot Volcanism on Venus from VIRTIS Emissivity Data. Science 328, 605. doi:10.1126/science.1186785

Solem, J. C. 1995. The Cometary breakup calculations based on a gravitationally-bound agglomeration model: the density and size of Shoemaker-Levy 9. Astronomy and Astrophysics, v.302, p.596-608

Spencer, J. R. and 6 colleagues 2005. Mid-infrared detection of large longitudinal asymmetries in Io's SO_2 atmosphere. Icarus 176, 283-304. doi:10.1016/j.icarus.2005.01.019

Sprague, A. L., Bjoraker, G. L., Hunten, D. M., Wittenborn, F. C., Kozlowski, R. W. H., Wooden, D. H. 1996. Water Brought into Jupiter's Atmosphere by Fragments R and W of Comet SL-9. Icarus 121, 30-37. doi:10.1006/icar.1996.0069

Teanby, N. A., Irwin, P. G. J. 2013. An External Origin for Carbon Monoxide on Uranus from Herschel/SPIRE?. The Astrophysical Journal 775. doi:10.1088/2041-8205/775/2/L49

Tinetti, G., Encrenaz, T., Coustenis, A. 2013. Spectroscopy of planetary atmospheres in our Galaxy. Astronomy and Astrophysics Review 21. doi:10.1007/s00159-013-0063-6

Tokunaga, A. T., Knacke, R. F., Ridgway, S. T. 1980. High spatial and spectral resolution 10-μm observations of jupiter. Icarus 44, 93-101. doi:10.1016/0019-1035(80)90058-5

Trafton, L. M., Geballe, T. R., Miller, S., Tennyson, J., Ballester, G. E. 1993. Detection of H_3^+ from Uranus. The Astrophysical Journal 405, 761. doi:10.1086/172404

Tsang, C. C. C., Spencer, J. R., Lellouch, E., Lopez-Valverde, M. A., Richter, M. J., Greathouse, T. K. 2012. Io's atmosphere: Constraints on sublimation support from density variations on seasonal timescales using NASA IRTF/TEXES observations from 2001 to 2010. Icarus 217, 277-296. doi:10.1016/j.icarus.2011.11.005

1523 Tsang, C. C. C., Spencer, J. R., Jessup, K. L. 2013. Synergistic observations of Io's atmosphere
1524 in 2010 from HST-COS in the mid-ultraviolet and IRTF-TEXES in the mid-infrared. Icarus 226,
1525 604-616. doi:10.1016/j.icarus.2013.06.010

1526 Usui, T., Alexander, C. M. O., Wang, J., Simon, J. I., Jones, J. H. 2012. Origin of water and
1527 mantle-crust interactions on Mars inferred from hydrogen isotopes and volatile element
1528 abundances of olivine-hosted melt inclusions of primitive shergottites. Earth and Planetary
1529 Science Letters 357, 119-129. doi:10.1016/j.epsl.2012.09.008

1530 Villanueva, G. L. and 8 colleagues 2015. Strong water isotopic anomalies in the Martian
1531 atmosphere: Probing current and ancient reservoirs. Science 348, 218-221.
1532 doi:10.1126/science.aaa3630

1533 Webster, C. R. and 569 colleagues 2015. Mars methane detection and variability at Gale
1534 crater. Science 347, 415-417. doi:10.1126/science.1261713

1535 Webster, C. R. and 12 colleagues 2021. Day-night differences in Mars methane suggest
1536 nighttime containment at Gale crater. Astronomy and Astrophysics 650. doi:10.1051/0004-
1537 6361/202040030

1538 Zasova, L. V., Moroz, V. I., Esposito, L. W., Na, C. Y. 1993. SO_2 in the Middle Atmosphere of
1539 Venus: IR Measurements from Venera-15 and Comparison to UV Data. Icarus 105, 92-109.
1540 doi:10.1006/icar.1993.1113

1541 Zhang, X., Liang, M.-C., Montmessin, F., Bertaux, J.-L., Parkinson, C., Yung, Y. L. 2010.
1542 Photolysis of sulphuric acid as the source of sulphur oxides in the mesosphere of Venus.
1543 Nature Geoscience 3, 834-837. doi:10.1038/ngeo989

1544 Zhang, X., Liang, M. C., Mills, F. P., Belyaev, D. A., Yung, Y. L. 2012. Sulfur chemistry in the
1545 middle atmosphere of Venus. Icarus 217, 714-739. doi:10.1016/j.icarus.2011.06.016